



Yasser Chiker · Mourad Bachene · Brahim Attaf ·
Ahmed Hafaifa · Mouloud Guemana

Uncertainty influence of nanofiller dispersibilities on the free vibration behavior of multi-layered functionally graded carbon nanotube-reinforced composite laminated plates

Received: 7 August 2022 / Revised: 26 September 2022 / Accepted: 7 November 2022 / Published online: 7 January 2023
© The Author(s), under exclusive licence to Springer-Verlag GmbH Austria, part of Springer Nature 2023

Abstract Uncertainties caused by the deviation of functionally graded reinforcements from the ideal linear distribution form are unavoidable during the manufacturing process, and this can significantly influence the vibrational behavior of carbon-based nanocomposite plates. In this context, this work aims to carry out a detailed parametric study on the free vibration response of laminated composite plates made of multi-layer carbon-based nanocomposite plies, considering both linear and nonlinear distribution forms of the nano-reinforcements. Materials constituting the plies are nano-reinforcement-based carbon nanotubes (CNTs) embedded in a polymer matrix. The CNTs are assumed to be either uniformly distributed (UD) or functionally graded (FG) across the ply thickness. Two types of laminated plate arrangements are comparatively investigated. The effective material properties such as elastic modulus and mass density are derived using the extended rule of mixture, whereas the governing equations are obtained through the combination of the Lagrange equation of motion and the first-order shear deformation theory (FSDT). The natural frequencies of the carbon nanotube-reinforced composite (CNTRC) laminated plates are obtained using the finite element method. The accuracy of the present numerical model is validated by comparing our results with those published in the open literature. The obtained numerical results show that both the plate layout arrangement and how the CNT fillers are dispersed along the ply thickness have a remarkable influence on the CNTRC laminated plates.

1 Introduction

In light of their utility and importance in aerospace, marine, automotive, and many other fields, nano-reinforcements are currently being thoroughly studied. This class of materials has admirable properties, including high fracture toughness, low weight, and relatively high strength [1], that make them highly desirable for such applications. Recent research work in this field has not only focused on the interface and structural morphology, and the determination of effective mechanical properties of nano-reinforcements but also on their architecture to help design functional composite materials using Artificial intelligence (AI) technology [2].

Y. Chiker · M. Bachene (✉)

Laboratory of Mechanics, Physics, Mathematical Modeling (LMP2M), University of Medea, 26000 Medea, Algeria
e-mail: bachene.mourad@univ-medea.dz

B. Attaf

Freelance Researcher in the Field of Composite Materials and Structures, 13013 Marseille, France

A. Hafaifa

Applied Automation and Industrial Diagnostics Laboratory, Faculty of Science and Technology, University of Djelfa, 17000 Djelfa, DZ, Algeria

A. Hafaifa

Department of Electrical and Electronics Engineering, Nisantasi University, 34398, Sariyer Istanbul, Turkey

M. Guemana

Laboratory of Applied Automation and Industrial Diagnostic (LAADI), University of Medea, Medea, Algeria

Due to their exceptional mechanical, thermal, and electrical properties, CNTs are considered to be an excellent candidate for the reinforcement of polymer composites [3–6], used in many applications ranging from marine and aerospace structures to the high technology of nuclear plants [7]. The combination of CNTs and polymer matrix (i.e., carbon nanotube-reinforced composite (CNTRC)) leads to composite structural components in the form of beams, plates, and shells to gain higher stiffness and strength coupled with a lower weight, which can be four times less for an equivalent cross section made of metallic materials [8, 9]. It has been reported in [10, 11] that the dispersion of low concentrated CNTs into polymeric matrices can remarkably enhance their mechanical properties. For instance, Qian et al. [12] found that mixing polystyrene with a 1% weight fraction of multi-walled carbon nanotubes (MWCNTs) can enhance the neat polystyrene in the elastic modulus of 36–42%. Moreover, many reported research works have noted that dispersing nano-reinforcements such as CNTs in a non-uniform fashion following kind patterns leads to improve mechanical properties of nanocomposite structures. In this context, an excellent review was reported by Liew et al. [13] on recent advances in functionally graded carbon nanotube-reinforced composite (FG-CNTRC) structures.

Recently, many of studies on the mechanical analysis of plates, shells, and beams made from functionally graded materials (FGMs) have been published in the literature [14–18]. In such research works, FGMs are generally characterized by a gradual variation of compositions (typically ceramic and metal) and mechanical properties to achieve the required performance criteria.

Using the FGM concept, Shen [19] first addressed an analysis of the CNT-based FGM to study the nonlinear bending behavior of FG-CNT-reinforced composite plates in thermal environments. Since then, a large number of works have been reported to investigate the effect of CNT volume fraction and their distribution patterns together with other influencing factors, including: (i) dynamic analysis [20], (ii) static analysis [21, 22], (iii) buckling analysis [23, 24] and (iv) post-buckling analysis [25]. Additionally, the vibrational response has been analyzed for FG-CNTs reinforced composite elliptical plates [26], circular plate [27], triangular plates [28], skew plates [29, 30], quadrilateral plates [31], shell plates [32, 33], arbitrary-shaped plates [34], sandwich plates [35, 36] and laminated plates [37].

The most-reported works in terms of investigating the mechanical behavior of FG-CNT composites deal only with the linear form of the distributed nanofillers across the thickness direction of the plate structures. On the one hand, this may lead to an incorrect numerical prediction, because during manufacturing processes, carbon nanotubes, may not disperse in a perfectly linear form, which causes uncertainty in the distribution of CNTs [38, 39]. And, on the other hand, this nonconformity may also lead to limitations in maximizing the overall strength and the high potential for using carbon-based nanocomposite structures. In this area of research, only a limited number of researchers have studied the influence of the uncertainty in the distribution patterns of the nano-reinforcements (i.e., the nonlinear dispersion of the nanofillers). In this context, Mirjavad et al. [40] studied the nonlinear free/forced vibration of FG graphene platelets (FG-GPL) reinforced microbeam employing the couple stress theory; in this study, the nanofillers are assumed to be either uniformly distributed or linearly and nonlinearly functionally graded along the thickness direction of the structure. From the results obtained, it was concluded that the lowest and highest vibration frequencies were obtained in the case of linear and nonlinear dispersion of GPL, respectively. However, Vo-Duy et al. [41] examined the static, free vibration, and buckling analyses of FG-CNT-reinforced composite beams using third-order shear deformation theory (TSDT). In this study, a type of novel nonlinear distribution of the FG-CNT was used to improve the stiffness of the structural beams. The Authors concluded that the dispersion of the CNT closer to the bottom and top surfaces of the beam structures makes it stiffer. Successfully, Tornabene et al. [42] investigated the effect of agglomeration on the natural frequencies of FG-CNT laminated composite doubly curved shells using the generalized differential quadrature method (GDQM); they considered various laminations schemes and several CNT exponential distributions across the thickness of the structures; the presented applications have proven that the presence of CNTs, in terms of both concentration and mass fraction, affects the stiffness of the structure. The same observations were made by Fantuzzi et al. [43] by studying the free vibration behavior of arbitrarily shaped FG-CNT-reinforced composite plates using the GDQ method. While, Jiao et al. [44] studied the effects of the uncertainty in the distributions of CNTs as well as their volume fractions on the buckling behavior of thin rectangular FG-CNT-reinforced composite plate subjected to an arbitrarily distributed partial edge compression loads. Their research results show that the critical buckling load of the CNTRC plates is affected by the uncertainty in the grading of CNT from one type of distribution to another. Using the FSDT, Garcia et al. [45] compared the bending and free vibration analysis of FG graphene versus carbon nanotube-reinforced composite plates. It has been found that the best way to improve the structure's stiffness is to disperse more nanofillers near the bottom and top surfaces of the structure. The same remarks were made by Chiker et al. [46] when investigating the free vibration behavior of functionally graded carbon-based

nanofillers, including CNT and GPL, using the FSDT. In their study, the CNT's volume fraction was assumed to be piece-wise functionally graded across the plate thickness employing a layer-wise formulation model. Based on the same methodology, Chiker et al. [47] studied the effect of the uncertainty in the grading profile for the vibrational behavior of hybrid laminated plates containing CNTRC plies. The reported results have proven that the configuration of the laminated plate structures with a special layout arrangement using the CNT distribution patterns can remarkably enhance its performance indices in terms of specific strength and/or specific stiffness.

Recently, the mechanical behavior of various laminated FG-CNTRC structures has been investigated under several influencing parameters, including CNT volume fractions, distribution patterns, plate geometry, number of layers, boundary conditions, and lamination sequences. In this subject area, Tran et al. [48] examined the static analysis of smart laminated CNTRC plates integrated with a piezoelectric layer employing a new four-variable refined plate theory. Using the FSDT and the meshless kp-Ritz method, Lei et al. [49] investigated the buckling behavior of FG-CNT-reinforced composite laminated plate. Employing the higher-order shear deformation theory (HSDT) together with Hamilton's principle, Chakraborty et al. [50] studied the stability and vibration analyses of FG-CNT-reinforced composite laminated cylindrical shell panels. Moreover, Arani et al. [51] presented the free and forced vibration analyses of multi-layered FG composite cylindrical panels reinforced with single-wall CNTs using the Reddy's TSDT and Hamilton's principle. Furthermore, Nguyen-Quang et al. [52] investigated the dynamic response of FG-CNT-reinforced composite laminated plates integrated with piezoelectric layers using the HSDT. While Fu et al. [53] carried out the static and free vibration analyses of laminated FG-CNT-reinforced composite rectangular plates on an elastic foundation employing n th-order shear deformation theory and Hamilton's principle. Using both Maxwell's equation and Hamilton's principle, Tran et al. [54] investigated the free vibration analysis of smart laminated FG-CNT-reinforced composite plates integrated with a piezoelectric layer. Employing the FSDT and differential quadrature method, Malekzadeh et al. [55] studied the free vibration behavior of quadrilateral laminated thin-to-moderately thick plates with CNT-reinforced composite layers. The static and free vibration analyses of FG-CNT-reinforced composite laminated plates using a semi-analytical approach based on a layer-wise-differential quadrature method were examined by Malekzadeh and Heydarpour [56]. Whereas, Zhang and Selim [57] studied the vibration analysis of FG-CNT-reinforced composite thick laminated plates employing the Reddy's HSDT and element-free IMLS-Ritz method, where the Mori-Tanaka approach was employed to obtain the effective material properties. Using the FSDT and kp-Ritz method, Lei et al. [58] conducted the free vibration behavior of laminated FG-CNT-reinforced composite thin-to-moderately thick plates. Likewise, the free vibration and bending analyses of antisymmetrically laminated CNT-reinforced FG plates using the four-variable theory and Hamilton's principle were investigated by Huang et al. [59].

A literature survey on the background of the present work has been carefully introduced. The review revealed that several recent valuable studies on the analysis of FG-CNTRC had been performed. Nevertheless, it is relevant to examine some novel aspects that can affect the mechanical behavior of carbon-based nanocomposite structures. The literature review reveals the lack of existing studies on the matter of the effect of the uncertainty in the distribution of the nano-reinforcements on the specific stiffness and strength of FG-CNT-reinforced composite. Aiming to fill this gap, the present paper investigates the effect of linear and nonlinear distribution forms of CNT reinforcements on the free vibration behavior of nanocomposite laminated plates using the frameworks of a FEM.

In this article, two types of laminated plate configurations are considered and compared in terms of the layout arrangement of CNT distribution patterns. The effective mechanical properties of the nanocomposite are derived using the extended rule of mixture. Both the FSDT and Lagrange's equations are employed to obtain the governing equations. In addition, various illustrative results are provided to highlight the effects of (i) CNT distribution patterns, (ii) uncertainty in the distribution of CNTs, (iii) plate configurations, (iv) number of plies constituting the plate thickness, (v) CNT volume fraction, (vi) plate width/thickness and length/width ratios, (vii) CNTs orientation angle and (viii) plate boundary conditions on the natural frequencies of the CNTRC laminated plates.

2 Theoretical formulations and field equations

2.1 Geometrical and mechanical characterization

The structure under consideration is a perfectly bonded laminated multi-layer FG-CNT-reinforced composite plate with a total thickness h , width b , and length a (see Fig. 1a). The laminated plates contain n plies of

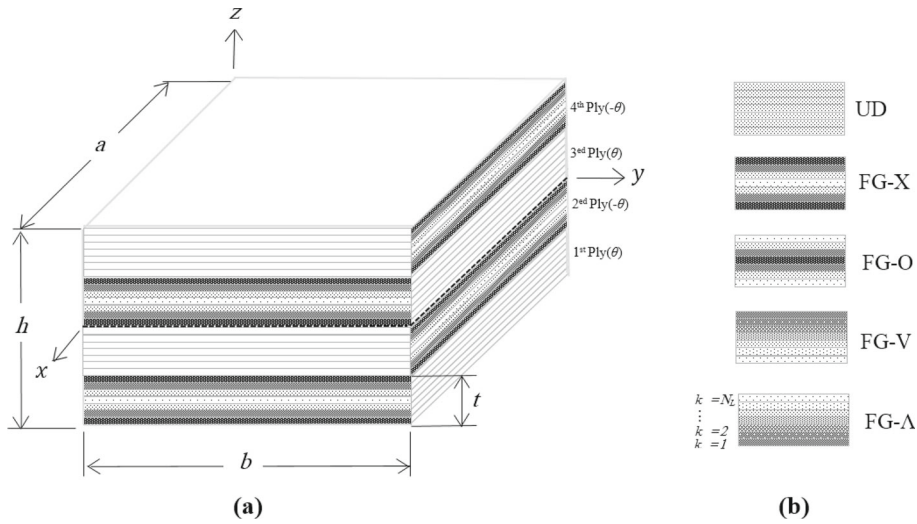


Fig. 1 Schematic of: **a** a laminated composite plate made from multi-layer CNTRC plies; **b** different distribution patterns of CNT fillers

multi-layer CNTRC. Assuming that each ply of the CNTRC laminated plate is divided into N_L layers, the ply thickness is given by $(t = \Delta h \times N_L)$, in which Δh is the thickness of each individual layer. The CNTRC plies are made of a polymeric material reinforced with CNTs. Taking into account the functionally graded and uniform distributions form of the CNTs, five different patterns are considered in the present study, with the following abbreviations identifying them: FG-V, FG- Λ , FG-O, FG-X, and UD, as illustrated in Fig. 1b. The CNT volume fraction (f_{CNT}) is assumed to change from layer-to-layer along the ply thickness (in layer-wise form) to provide the functionally graded dispersion. Accordingly, the CNT volume fraction in the k -th ply layer ($f_{CNT}^{(k)}$) for the considered distribution patterns are given as follows [46]:

$$UD : f_{CNT}^{(k)} = f_{CNT}^* \tag{1a}$$

$$FG - \Lambda : f_{CNT}^{(k)} = (1 + P_{in}) \left(\frac{(0.5 - k + N_L)}{N_L} \right)^{P_{in}} f_{CNT}^* \tag{1b}$$

$$FG - V : f_{CNT}^{(k)} = (1 + P_{in}) \left(\frac{k - 0.5}{N_L} \right)^{P_{in}} f_{CNT}^* \tag{1c}$$

$$FG - X : f_{CNT}^{(k)} = (1 + P_{in}) \left(\frac{|2k - N_L - 1|}{N_L} \right)^{P_{in}} f_{CNT}^* \tag{1d}$$

$$FG - O : f_{CNT}^{(k)} = (1 + P_{in}) \left(1 - \frac{|2k - N_L - 1|}{N_L} \right)^{P_{in}} f_{CNT}^* \tag{1e}$$

in which $k = 1, 2, 3 \dots N_L$. The P_{in} is the power-law index that sets out the uncertainty in the distribution of the nano-reinforcements, and f_{CNT}^* is the total volume fractions of CNTs. This latter is expressed as follows:

$$f_{CNT}^* = \frac{w_{CNT}}{w_{CNT} + (1 - w_{CNT})(\rho_{CNT} / \rho_m)}, \tag{2}$$

where w_{CNT} is the weight fraction of the CNTs; ρ_{CNT} and ρ_m are the CNT and matrix mass density, respectively. The subscripts “CNT” and “m” are referred to as the carbon nanotube and polymer matrix, respectively. In order to make a meaningful comparison, the total volume fraction of CNT (f_{CNT}^*) is kept constant for the five considered FG-CNT patterns.

According to the rule of mixture, the volume fraction of the polymer matrix is given as follows:

$$f_m^{(k)} = 1 - f_{CNT}^{(k)}. \tag{3}$$

Based on the extended rule of mixture micromechanics model [60], the effective elastic properties of the k -th CNTRC ply layer can be expressed as follows [61]:

$$E_{11}^{(k)} = f_{\text{CNT}}^{(k)} \eta_1 E_{11}^{\text{CNT}} + E_m (1 - f_{\text{CNT}}^{(k)}) \tag{4}$$

$$E_{22}^{(k)} = \frac{\eta_2}{\frac{f_{\text{CNT}}^{(k)}}{E_{22}^{\text{CNT}}} + \frac{(1-f_{\text{CNT}}^{(k)})}{E_m}} \tag{5}$$

$$G_{12}^{(k)} = \frac{\eta_3}{\frac{f_{\text{CNT}}^{(k)}}{G_{12}^{\text{CNT}}} + \frac{(1-f_{\text{CNT}}^{(k)})}{G_m}} \tag{6}$$

In Eqs. (4–6), elastic and shear moduli of the polymeric CNT-reinforced-composite are characterized by E_{11}^{CNT} , E_{22}^{CNT} , G_{12}^{CNT} and E_m , G_m , respectively, while η_i ($i = 1,2,3$) are the CNT/matrix efficiency parameters, which are introduced to deal with the small scale effect [4, 62].

Using the rule of mixture, the effective Poisson’s ratio and mass density are expressed as follows [63]:

$$\rho^{(k)} = f_{\text{CNT}}^{(k)} \rho^{\text{CNT}} + (1 - f_{\text{CNT}}^{(k)}) \rho_m \tag{7}$$

$$\nu_{12}^{(k)} = f_{\text{CNT}}^* \nu_{12}^{\text{CNT}} + (1 - f_{\text{CNT}}^{(k)}) \nu_m \tag{8}$$

where ν_m and ν_{12}^{CNT} are the Poisson’s ratios of matrix and CNT, respectively.

Figure 2 shows the variation of the CNT volume fraction ratios ($f_{\text{CNT}}^{(k)} / f_{\text{CNT}}^*$) across the thickness direction of a single ply of CNTRC plate with different FG-CNT patterns, including UD, FG-V, FG- Λ , FG-X, and FG-O patterns. As can be seen from Fig. 2, the CNT reinforcements follow three forms of distribution across the thickness of the plate, notably: (i) the uniform distribution form ($P_{\text{in}} = 0$), (ii) the linear distribution form ($P_{\text{in}} = 1$), and (iii) the nonlinear distribution form ($P_{\text{in}} \neq 0$ and 1). Since the CNT volume fraction (1) decreases from the bottom and top layers to the mid-layers for the FG-X pattern, (2) increases from the top and bottom layers to the mid-layers for the FG-O pattern, (3) decreases from the top to the bottom layers for FG-V pattern, and (4) increases from the top to the bottom layers for FG- Λ pattern, the volume fraction ratio as a function of the thickness direction ratio (z/h) varies in a symmetric way for both FG-X and FG-O patterns and in an unsymmetrical way for FG-V and FG- Λ patterns, as shown in Fig. 2a–d.

A comparison of frequency parameters of two laminated plate configurations is performed, and the plates arrangement depends on the distribution patterns that contain, namely Configuration-I and Configuration-II, (see Fig. 3). For both configurations, laminated plates have four plies of CNTRC. In Configuration-I, the laminated plates contain FG-X distribution patterns, and in Configuration-II the laminated plates contain a combination of FG- Λ and FG-V patterns which are located in the lower and the upper half of the laminated plate, respectively.

2.2 Governing equations of the CNTRC laminated plate

The displacement fields of any point M (x, y, z) in the laminated plate are obtained by using the first-order shear deformation theory (FSDT) [64]:

$$\begin{Bmatrix} u(x, y, z) \\ v(x, y, z) \\ w(x, y, z) \end{Bmatrix} = \begin{Bmatrix} u_0(x, y) \\ v_0(x, y) \\ w_0(x, y) \end{Bmatrix} + z \begin{Bmatrix} \theta_x(x, y) \\ \theta_y(x, y) \\ 0 \end{Bmatrix}, \tag{9}$$

in which $u_0(x, y)$, $v_0(x, y)$ and $w_0(x, y)$ are the translational displacements of a point (x, y) at the mid-plane of the laminated plate; $\theta_y(x, y)$ and $\theta_x(x, y)$ denote the rotations of the transverse normal about the x and y axes, respectively.

According to the FSDT, strain and displacement relationships are expressed as:

$$\begin{Bmatrix} \varepsilon_{xx} \\ \varepsilon_{yy} \\ \gamma_{xy} \end{Bmatrix} = \varepsilon_0 + z\kappa, \quad \begin{Bmatrix} \gamma_{yz} \\ \gamma_{xz} \end{Bmatrix} = \gamma_0, \tag{10}$$

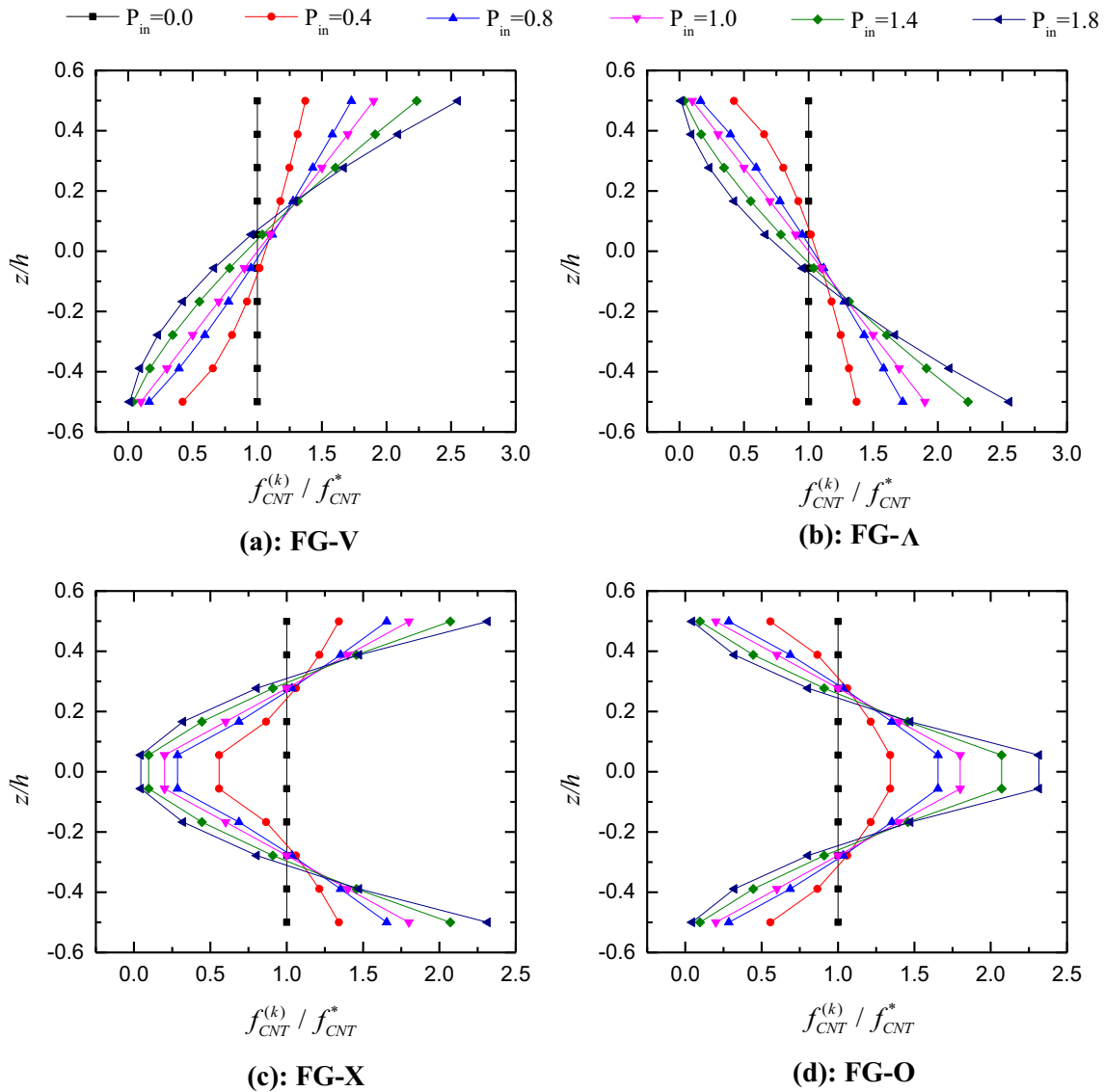


Fig. 2 Variation of CNT volume fraction ratio along the thickness direction ratio for plates with: **a** FG-V, **b** FG-Λ, **c** FG-X and **d** FG-O patterns

where

$$\epsilon_0 = \begin{Bmatrix} \frac{\partial u_0}{\partial x} \\ \frac{\partial v_0}{\partial y} \\ \frac{\partial u_0}{\partial y} + \frac{\partial v_0}{\partial x} \end{Bmatrix}, \quad \kappa = \begin{Bmatrix} \frac{\partial \theta_x}{\partial x} \\ \frac{\partial \theta_y}{\partial y} \\ \frac{\partial \theta_x}{\partial y} + \frac{\partial \theta_y}{\partial x} \end{Bmatrix}, \quad \gamma_0 = \begin{Bmatrix} \theta_y + \frac{\partial w_0}{\partial y} \\ \theta_x + \frac{\partial w_0}{\partial x} \end{Bmatrix}. \tag{11}$$

The stress–strain relationship for the *k*-th layer of the CNTRC ply is given as:

$$\begin{Bmatrix} \sigma_x \\ \sigma_y \\ \tau_{xy} \\ \tau_{yz} \\ \tau_{xz} \end{Bmatrix}^{(k)} = \begin{bmatrix} Q_{11} & Q_{12} & 0 & 0 & 0 \\ Q_{12} & Q_{22} & 0 & 0 & 0 \\ 0 & 0 & Q_{66} & 0 & 0 \\ 0 & 0 & 0 & Q_{44} & 0 \\ 0 & 0 & 0 & 0 & Q_{55} \end{bmatrix}^{(k)} \begin{Bmatrix} \epsilon_x \\ \epsilon_y \\ \epsilon_{xy} \\ \epsilon_{yz} \\ \epsilon_{xz} \end{Bmatrix}^{(k)}, \tag{12}$$

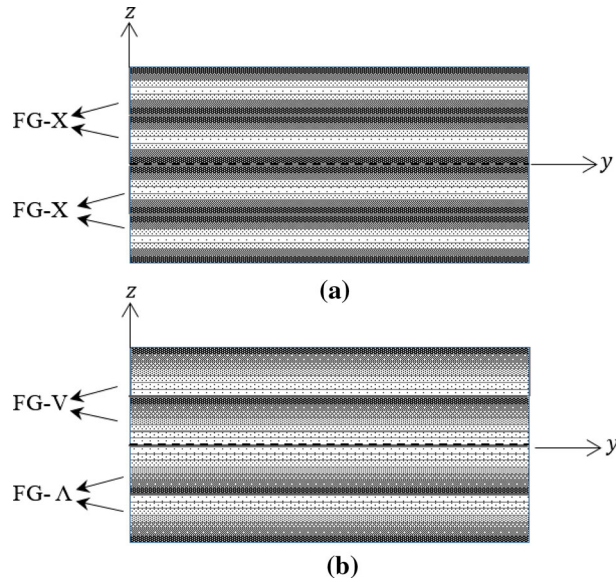


Fig. 3 Configuration types of the CNTRC laminated plates: **a** Configuration-I; **b** Configuration-II

where

$$Q_{11}^{(k)} = \frac{E_{11}^{(k)}}{1 - \nu_{12}^{(k)} \nu_{21}^{(k)}}, \quad Q_{12}^{(k)} = \frac{\nu_{21}^{(k)} E_{11}^{(k)}}{1 - \nu_{12}^{(k)} \nu_{21}^{(k)}}, \quad Q_{22}^{(k)} = \frac{E_{22}^{(k)}}{1 - \nu_{12}^{(k)} \nu_{21}^{(k)}}, \quad Q_{44}^{(k)} = G_{23}^{(k)}, \quad Q_{55}^{(k)} = G_{13}^{(k)}, \quad Q_{66}^{(k)} = G_{12}^{(k)}. \tag{13}$$

The axial forces (N_x, N_y, N_{xy}), moment resultants (M_x, M_y, M_{xy}) and shear forces (Q_x, Q_y) are related to the strain components by:

$$\begin{Bmatrix} N_x \\ N_y \\ N_{xy} \end{Bmatrix} = \begin{bmatrix} A_{11} & A_{12} & A_{16} \\ A_{12} & A_{22} & A_{26} \\ A_{16} & A_{26} & A_{66} \end{bmatrix} \varepsilon_0 + \begin{bmatrix} B_{11} & B_{12} & B_{16} \\ B_{12} & B_{22} & B_{26} \\ B_{16} & B_{26} & B_{66} \end{bmatrix} \kappa, \tag{14a}$$

$$\begin{Bmatrix} M_x \\ M_y \\ M_{xy} \end{Bmatrix} = \begin{bmatrix} B_{11} & B_{12} & B_{16} \\ B_{12} & B_{22} & B_{26} \\ B_{16} & B_{26} & B_{66} \end{bmatrix} \varepsilon_0 + \begin{bmatrix} D_{11} & D_{12} & D_{16} \\ D_{12} & D_{22} & D_{26} \\ D_{16} & D_{26} & D_{66} \end{bmatrix} \kappa, \tag{14b}$$

$$\begin{Bmatrix} Q_y \\ Q_x \end{Bmatrix} = k_s \begin{bmatrix} F_{44} & F_{45} \\ F_{45} & F_{55} \end{bmatrix} \gamma_0, \tag{14c}$$

in which k_s is the shear correction factor, and the value k_s is taken as 5/6 in this analysis. The stiffness elements A_{ij}, B_{ij}, D_{ij} and F_{ij} of the ply are defined as follows:

$$(A_{ij}, B_{ij}, D_{ij}) = \sum_{k=1}^n \int_{Z_k}^{Z_{k+1}} Q_{ij}^{(k)}(1, z, z^2) dz, \quad (i, j = 1, 2, 6) \tag{15}$$

and

$$F_{ij} = \sum_{k=1}^n \int_{Z_k}^{Z_{k+1}} Q_{ij}^{(k)} dz, \quad (i, j = 4, 5). \tag{16}$$

Equations (14) can be written in compact matrix form as follows:

$$\begin{Bmatrix} N \\ M \\ Q \end{Bmatrix} = \begin{bmatrix} A & B & 0 \\ B & D & 0 \\ 0 & 0 & F \end{bmatrix} \begin{Bmatrix} \varepsilon_0 \\ \kappa \\ \gamma \end{Bmatrix}. \tag{17}$$

2.3 Finite element formulation

The numerical analysis in this work is performed based on a nine-node isoparametric quadrilateral element. Each node possesses five independent degrees of freedom (three displacements (i.e., u, v, w) and two rotations (i.e., θ_x, θ_y). Thus, the elementary displacement field can be written as:

$$\begin{Bmatrix} u_0 \\ v_0 \\ w_0 \\ \theta_x \\ \theta_y \end{Bmatrix} = \sum_{i=1}^9 \begin{bmatrix} N_i & 0 & 0 & 0 & 0 \\ 0 & N_i & 0 & 0 & 0 \\ 0 & 0 & N_i & 0 & 0 \\ 0 & 0 & 0 & N_i & 0 \\ 0 & 0 & 0 & 0 & N_i \end{bmatrix} \begin{Bmatrix} u_{0i} \\ v_{0i} \\ w_{0i} \\ \theta_{xi} \\ \theta_{yi} \end{Bmatrix}, \tag{18a}$$

in which N_i are the shape functions. Equation (18a) can also be expressed in a compact matrix form as follows:

$$\{\delta\} = [N]\{\delta_e\}. \tag{18b}$$

The relationship between the elementary strain and displacement is derived from Eq. (18) as

$$\begin{Bmatrix} \varepsilon_{0x} \\ \varepsilon_{0y} \\ \gamma_{0xy} \\ \kappa_x \\ \kappa_y \\ \kappa_{xy} \\ \gamma_{xz} \\ \gamma_{yz} \end{Bmatrix} = \sum_{i=1}^9 \begin{bmatrix} \partial N_i / \partial x & 0 & 0 & 0 & 0 \\ 0 & \partial N_i / \partial y & 0 & 0 & 0 \\ \partial N_i / \partial y & \partial N_i / \partial x & 0 & 0 & 0 \\ 0 & 0 & 0 & \partial N_i / \partial x & 0 \\ 0 & 0 & 0 & 0 & \partial N_i / \partial y \\ 0 & 0 & 0 & \partial N_i / \partial y & \partial N_i / \partial x \\ 0 & 0 & \partial N_i / \partial x & N_i & 0 \\ 0 & 0 & \partial N_i / \partial y & 0 & N_i \end{bmatrix} \begin{Bmatrix} u_{0i} \\ v_{0i} \\ w_{0i} \\ \theta_{xi} \\ \theta_{yi} \end{Bmatrix}, \tag{19a}$$

or in compact matrix form as

$$\{\varepsilon\} = [B]\{\varepsilon_e\}. \tag{19b}$$

According to the Lagrange equations and finite element discretization process, the equilibrium equation for free vibration behavior can be written as

$$[M]\{\ddot{\delta}\} + [K]\{\delta\} = \{0\}, \tag{20}$$

where $[K]$ and $[M]$ are, respectively, the global stiffness and global mass matrix, and $\{\ddot{\delta}\}$ and $\{\delta\}$ are the acceleration and nodal displacement vector, respectively.

$[M]$ and $[K]$ are obtained by assembling the elementary mass matrix $[M_e]$ and stiffness matrix $[K_e]$; these latter are expressed as follows:

$$[M_e] = \int_{\Lambda_e} [N]^T [\bar{m}] [N] d\Lambda_e, \tag{21}$$

$$[K_e] = \int_{\Lambda_e} [B]^T [C] [B] d\Lambda_e, \tag{22}$$

where Λ_e is the elementary surface, $[\bar{m}]$ is the inertia matrix and $[C]$ is the elasticity matrix; they are expressed as:

$$\bar{m} = \begin{bmatrix} I_0 & 0 & 0 & I_1 & 0 \\ 0 & I_0 & 0 & 0 & I_1 \\ 0 & 0 & I_0 & 0 & 0 \\ I_1 & 0 & 0 & I_2 & 0 \\ 0 & I_1 & 0 & 0 & I_2 \end{bmatrix}, C = \begin{bmatrix} A & B & 0 \\ B & D & 0 \\ 0 & 0 & F \end{bmatrix}, \tag{23}$$

in which $I_i = \sum_{k=1}^n \int_{z_{k-1}}^{z_k} z^i \rho^k dz, i = 0,1,2$ and ρ^k is the material density of the k th ply layer.

Table 1 Material properties of the polymer matrix and (10,10) SWCNTs [19, 62]

Polymer matrix	(10,10) SWCNTs
$E_m = 2.1 \text{ GPa}$	$E_{11}^{\text{CNT}} = 5646.6 \text{ GPa}$
$\rho_m = 1150 \text{ kg/m}^3$	$E_{22}^{\text{CNT}} = 7080.0 \text{ GPa}$
$\nu_m = 0.34$	$G_{12}^{\text{CNT}} = 1944.5 \text{ GPa}$
	$\rho^{\text{CNT}} = 1400 \text{ kg/m}^3$
	$\nu_{12}^{\text{CNT}} = 0.175$

Table 2 CNT/matrix efficiency parameters [19]

f_{CNT}^*	η_1	η_2	η_3
0.11	0.149	0.934	0.934
0.14	0.150	0.941	0.941
0.17	0.149	1.381	1.381

3 Numerical applications

The numerical applications reported in this section are performed using an in-house finite element computer code, developed and maintained by our research team. Initially, the validity of the present approach is examined by comparing the achieved results with those reported in the literature; then, many applications and parametric studies, as shown in Sect. 1, are carried out.

The armchair (10,10) single-walled carbon nanotubes (SWCNTs) are selected as reinforcements, and the poly(m-phenylenevinylene)-co-[(2,5-dioctoxy-p-phenylene) vinylene] (PmPV) is selected as matrix. The mechanical properties of both constituent materials at a temperature of 300 K are listed in Table 1. The CNT/matrix efficiency parameters for three levels of CNT volume fractions are given in Table 2. It is assumed that $G_{12} = G_{13} = G_{23}$.

For the proposed applications, the plates are discretized into 8×8 elements and the following boundary conditions (BCs) are considered:

1. Simply supported edge (S):

Angle-ply laminate ($45^\circ/-45^\circ/45^\circ/-45^\circ$):

$$\begin{aligned} \text{at } x = 0, a: u_0 = w_0 = \theta_y = 0, \\ \text{at } y = 0, b: v_0 = w_0 = \theta_x = 0. \end{aligned}$$

cross-ply laminate ($0^\circ/90^\circ/0^\circ/90^\circ$):

$$\begin{aligned} \text{at } x = 0, a: v_0 = w_0 = \theta_y = 0, \\ \text{at } y = 0, b: u_0 = w_0 = \theta_x = 0. \end{aligned}$$

2. Clamped edge (C):

at $x = 0, a:$ and $y = 0, b: u_0 = v_0 = w_0 = \theta_x = \theta_y = 0$, for both angle-ply and cross-ply laminates.

Natural frequencies are expressed in non-dimensional form by using the following expression:

$$\bar{\omega} = \omega(b^2/h)\sqrt{\rho^m/E^m}. \tag{24}$$

3.1 Comparative studies

Three comparative studies are performed; the first one concerns the case of a functionally graded alumina/aluminum ($\text{Al}_2\text{O}_3/\text{Al}$) square simply supported plate. The mechanical properties of the Al_2O_3 and Al materials are given as follows [65]:

$$E_{\text{Al}_2\text{O}_3} = 380.0 \text{ GPa}, \quad \rho_{\text{Al}_2\text{O}_3} = 3800 \text{ kg/m}^3, \quad \nu_{\text{Al}_2\text{O}_3} = 0.3,$$

Table 3 Comparison of the first six non-dimensional natural frequency ($\bar{\omega} = \omega h \sqrt{\rho_{Al_2O_3}/E_{Al_2O_3}}$) of square FG (Al/Al₂O₃) plates ($b/h = 0.5$; $N_L = 10$; SSSS)

		Mode	P_{in}				
			0	0.5	1	4	10
Present	1		0.2112	0.1812	0.1631	0.1389	0.1308
Ref [65]			0.2121	0.1819	0.1640	0.1383	0.1306
Present	2		0.3897	0.3496	0.3232	0.2600	0.2287
Ref [65]			0.3874	0.3343	0.3020	0.2502	0.2300
Present	3		0.3897	0.3496	0.3232	0.2600	0.2287
Ref [65]			0.3897	0.3497	0.3236	0.2607	0.2337
Present	4		0.4618	0.3988	0.3598	0.3029	0.2825
Ref [65]			0.4658	0.4040	0.3644	0.3000	0.2790
Present	5		0.5515	0.4937	0.4556	0.3657	0.3224
Ref [65]			0.5511	0.4941	0.4567	0.3668	0.3243
Present	6		0.6673	0.5789	0.5232	0.4374	0.4054
Ref [65]			0.6566	0.5878	0.5325	0.4325	0.3855

$$E_{Al} = 70.0 \text{ GPa}, \quad \rho_{Al} = 2702 \text{ kg/m}^3, \quad \nu_{Al} = 0.3.$$

The effective material properties of the functionally graded Al₂O₃/Al plates are estimated using the following layer-wise formulation [46]:

$$E^{(k)} = (E_{Al_2O_3} - E_{Al}) \left(\frac{k - 0.5}{N_L} \right)^{P_{in}} + E_{Al}, \quad (25a)$$

$$\rho^{(k)} = (\rho^{Al_2O_3} - \rho_{Al}) \left(\frac{k - 0.5}{N_L} \right)^{P_{in}} + \rho_{Al}, \quad (25b)$$

$$\nu^{(k)} = 0.3. \quad (25c)$$

Herein, N_L is the number of plate layers and $k = 1, 2, 3 \dots N_L$.

Results in terms of non-dimensional frequencies, $\bar{\omega} = \omega h \sqrt{\rho_{Al_2O_3}/E_{Al_2O_3}}$, are presented in Table 3 and are compared with those reported by Matsunaga [65]. As can be observed from Table 3, the obtained results and those reported in Ref. [65] are in good agreement. In this analysis, the width/thickness ratio (b/h) and the number of ply layers (N_L) are set to 5 and 10, respectively.

For the second comparison study, a cross-ply ($0^\circ/90^\circ/0^\circ/90^\circ/0^\circ$) CNTRC square laminated plate is considered. The first six dimensionless frequencies, obtained for the different CNT distribution patterns (i.e., UD, FG-O, FG-V, and FG-X), are tabulated in Table 4 and are compared with the results published by Lie et al. [58]. The number of ply layers (N_L), width/thickness ratio (b/h), and CNT volume fraction (f_{CNT}^*) are selected to be 20, 10 and 0.14, respectively, whereas the SSSS and CCCC boundary conditions are used. The material properties are listed in Tables 1 and 2. By way of comparison, it can be seen that the obtained results are in good agreement with those given by Lie et al. [58], where the maximum percentage difference is about 2.32%.

The third comparison study concerns the case of a simply supported CNTRC square laminated plate with two cases of stacking sequences, namely $(0^\circ/90^\circ)_n$ and $(45^\circ/-45^\circ)_n$ where ($n = 1, 2$ and 3). The number of ply layers (N_L), width/thickness ratio (b/h) and CNT volume fraction (f_{CNT}^*) are chosen as 20, 50 and 0.14, respectively. As can be seen after comparison in Table 5, the obtained results agree well with those obtained by Hang et al. [59].

It can be concluded from the above comparative studies that the numerical model used in the present paper can provide accurate predictions for the free vibration of FG nanocomposite laminated plate structures.

3.2 Free vibration analysis of CNTRC laminated plates

3.2.1 Effect of the number of layers constituting the plies

To determine the minimum number of layers (N_L) constituting the plies, which can properly assess the desired distribution patterns of the nano-reinforcements through the ply thickness, a study on the convergence of

Table 4 Comparison of the first six non-dimensional natural frequencies $\bar{\omega} = \omega(b^2/h)\sqrt{\rho_m/E_m}$ of CNT-reinforced composite square laminated plates with $(0^\circ/90^\circ/0^\circ/90^\circ/0^\circ)$ stacking sequence ($f_{CNT}^* = 0.14$; $b/h = 10$; $a/b = 1$; $N_L = 20$)

BCs	Distribution patterns	Reference	Mode number						
			1	2	3	4	5	6	
SSSS	FG-O	Ref. [58]	15.213	19.850	19.855	28.566	31.800	39.691	
		Present	15.188 (0.16)	19.551 (1.51)	19.551 (1.53)	28.297 (0.94)	31.498 (0.95)	39.212 (1.21)	
	FG-V	Ref. [58]	15.248	19.850	19.855	28.634	31.824	39.691	
		Present	15.149 (0.65)	19.633 (1.09)	19.633 (1.12)	28.219 (1.45)	31.539 (0.90)	39.199 (1.24)	
	UD	Ref. [58]	15.270	19.761	19.767	28.666	31.747	39.514	
		Present	15.127 (0.94)	19.638 (0.62)	19.638 (0.65)	28.178 (1.70)	31.540 (0.65)	39.182 (0.84)	
	FG-X	Ref. [58]	15.397	19.850	19.855	28.922	31.924	39.691	
		Present	15.315 (0.53)	19.638 (1.07)	19.638 (1.09)	28.557 (1.26)	31.676 (0.78)	39.491 (0.50)	
	CCCC	FG-O	Ref. [58]	20.466	32.064	33.791	41.894	47.907	50.522
			Present	20.594 (-0.63)	31.931 (0.41)	33.762 (0.09)	41.264 (1.50)	46.979 (1.94)	49.372 (2.28)
		FG-V	Ref. [58]	20.499	32.116	33.888	41.999	48.002	50.702
			Present	20.617 (-0.58)	31.947 (0.53)	33.839 (0.14)	41.312 (1.64)	47.035 (2.01)	49.527 (2.32)
UD		Ref. [58]	20.475	32.079	33.868	41.966	47.953	50.686	
		Present	20.497 (-0.11)	31.834 (0.76)	33.731 (0.40)	41.219 (1.78)	47.022 (1.94)	49.525 (2.29)	
FG-X		Ref. [58]	20.601	32.281	33.973	42.141	48.219	50.772	
		Present	20.731 (-0.63)	32.151 (0.40)	33.947 (0.08)	41.512 (1.49)	47.282 (1.94)	49.618 (2.27)	

*Parenthesis values denote percentage errors with respect to the results available in Ref. [58]

Table 5 Comparison of the first natural frequency ($\bar{\omega} = \omega(b^2/h)\sqrt{\rho_m/E_m}$) of simply supported CNT-reinforced composite square laminated plates ($f_{CNT}^* = 0.14$; $b/h = 50$; $a/b = 1$; $N_L = 20$)

Staking sequences	n	FG-O	FG-V	UD			FG-X		
		Present	Ref. [59]	Present	Ref. [59]	Present	Ref. [59]	Present	Ref. [59]
$(0^\circ/90^\circ)_n$	1	9.973	9.874	10.952	10.876	12.386	12.395	14.418	14.396
	2	19.366	19.354	19.492	19.484	19.695	19.726	20.034	20.032
	4	21.030	21.036	21.058	21.065	21.100	21.142	21.185	21.193
$(45^\circ/-45^\circ)_n$	1	13.026	12.996	15.397	15.388	16.614	16.631	19.550	19.600
	2	26.489	26.536	26.660	26.694	26.950	27.005	27.421	27.481
	4	28.790	28.859	28.827	28.908	28.888	28.961	29.004	29.077

the first non-dimensional frequency parameter $\bar{\omega}$ versus the number of layers (N_L) constituting the plies is performed. Let us start with the case of a single ply CNTRC square plate with width/thickness ratio $b/h = 10$ and CNT volume fraction $f_{CNT}^* = 0.11$. The boundary conditions used for the plates investigated are either fully simply supported (SSSS) or fully clamped (CCCC). Three distribution patterns are considered, namely FG- Λ , FG-V, and FG-X. The analysis is performed for different power-law indexes ($P_{in} = 0, 0.4, 0.8, 1, 1.4, \text{ and } 1.8$). It can be seen from Fig. 4 that when $P_{in} = 0$, the fundamental non-dimensional frequency ($\bar{\omega}$) remains constant with the increase in N_L which occurs for all considered cases of distribution patterns. The physical reason for this matter is believed to be related to the fact that the CNTs are uniformly distributed across the ply thickness. Results also reveal that when $P_{in} \neq 0$, the frequency parameter $\bar{\omega}$ increases with the increase of N_L for the FG-X distribution type; whereas for the two other non-uniform distribution patterns (i.e., FG- Λ and FG-V), the frequency parameter $\bar{\omega}$ decreases. According to Figs. 4a and b, the convergence of the frequency parameter $\bar{\omega}$ shows a similar trend for both SSSS and CCCC boundary conditions. Moreover, Fig. 4 indicates that the fundamental non-dimensional frequency remains constant when $N_L \geq 20$. Therefore, for the upcoming applications, N_L will be set to 20.

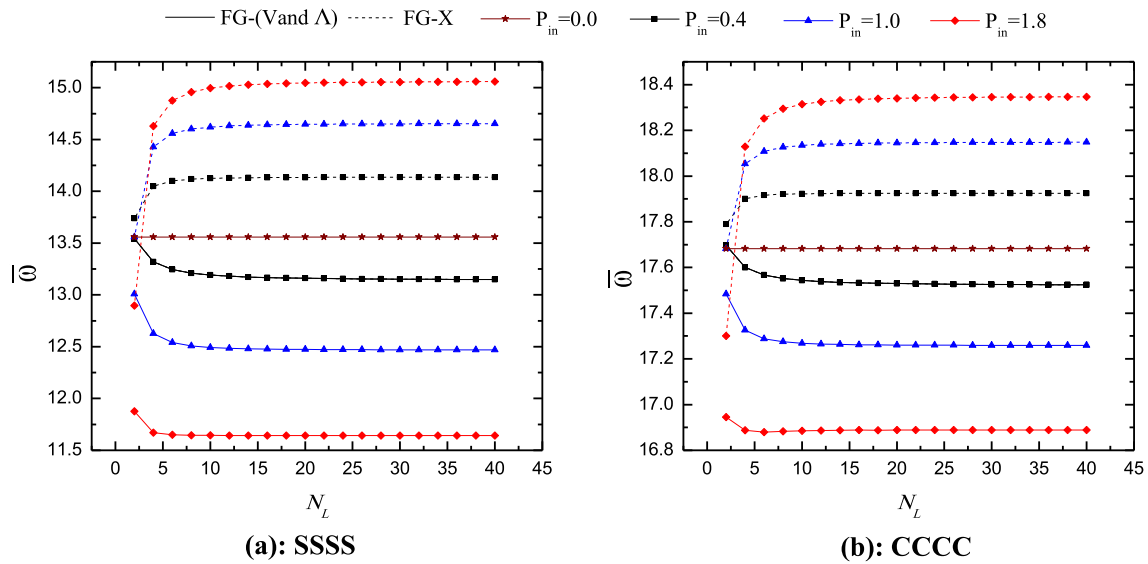


Fig. 4 Convergence of the first non-dimensional frequency $\bar{\omega}$ parameter versus the layer number of a single ply of CNTRC plates with different CNT distribution patterns, power-law indexes, and boundary conditions ($b/h = 10$; $a/b = 1$; $f_{\text{CNT}}^* = 0.11$)

3.2.2 Effects of plate width/thickness ratio and CNT volume fraction

The combined influences of the plate configuration, CNT volume fraction, power-law index, and plate width/thickness ratio on the fundamental non-dimensional, frequency ($\bar{\omega}$) parameter of the SSSS cross-ply ($0^\circ/90^\circ/0^\circ/90^\circ$) laminated plate are reported in Table 6. Two configurations for the stratification of plies with respect to the CNT distribution patterns are proposed, namely (a) Configuration-I: [X-X-X-X] and (b) Configuration-II: [Λ - Λ -V-V] as shown in Fig. 3. Table 6 shows that for a fixed value of P_{in} , the $\bar{\omega}$ parameter increases whenever the CNT volume fraction is added. Also, one can see that by increasing the width/thickness ratio, the value of $\bar{\omega}$ increases for both types of plate configurations. Results also indicate that the frequencies obtained with Configuration-II are higher than those obtained with Configuration-I with a value of $P_{\text{in}} \neq 0$. Table 7 presents the results of the first non-dimensional frequency of simply supported CNTRC laminated plate for an angle-ply stacking sequence ($45^\circ/-45^\circ/45^\circ/-45^\circ$). The results indicate that the fundamental frequencies of the angle-ply CNTRC laminated plates are affected by the width/thickness ratio, plate configuration, and CNT volume fraction in the same way as the cross-ply CNTRC laminated plates were affected.

3.2.3 Effects of plate length/width ratio and CNT volume fraction

The effect of CNT volume fraction associated with the effects of plate length/width ratio, power-law index, and plate configuration on the non-dimensional fundamental frequency ($\bar{\omega}$) of a simply supported cross-ply ($0^\circ/90^\circ/0^\circ/90^\circ$) CNTRC laminated plate are reported in Table 8, where b/h is taken equal to 10. It is observed that for a fixed value of P_{in} , the parameter $\bar{\omega}$ increases once the CNT volume fraction increases for the three values of length/width ratio considered, i.e., 2.0, 1.5, 1.0. For both types of plate configurations (I and II), the parameter $\bar{\omega}$ decreases when a/b increases. Also, it is evident that the values of $\bar{\omega}$ obtained with configuration-I are smaller than the ones obtained with configuration-II having $P_{\text{in}} \neq 0$. However, this advance is only provided when a/b is equal to 1 and 1.5. In other words, when a/b is equal to 2, the parameter $\bar{\omega}$ for both types of plate configurations (I and II) is nearly identical. Likewise, Table 9 presents the non-dimensional fundamental frequency ($\bar{\omega}$) of simply supported angle-ply ($45^\circ/-45^\circ/45^\circ/-45^\circ$) CNTRC laminated plates. One can conclude that for different values of CNT volume fractions, width/thickness ratios, and plate configurations, the parameter $\bar{\omega}$ of the angle-ply and cross-ply CNTRC laminated plates is affected in the same manner.

3.2.4 Effect of power-law index

Regarding the influence of the power-law index (P_{in}) that describes the nano-reinforcements dispersion through the ply thickness, or in other words, the parameter that describes uncertainty in the grading nano-reinforcements

Table 6 First non-dimensional frequency ($\bar{\omega} = \omega(b^2/h)\sqrt{\rho_m/E_m}$) of cross-ply (0°/90°/0°/90°) simply supported CNTRC laminated plates with different power-law indexes, plate configurations, CNT volume fractions, and width/thickness ratios ($a/b = 1$)

f_{CNT}^*	b/h	Plate configuration	P_{in}					
			0	0.4	0.8	1.0	1.4	1.8
0.11	10	Configuration-I	14.359	14.454	14.512	14.538	14.586	14.629
		Configuration-II	14.359	14.980	15.403	15.569	15.839	16.053
	20	Configuration-I	16.740	16.880	16.963	16.999	17.065	17.122
		Configuration-II	16.740	17.694	18.361	18.627	19.064	19.410
0.14	10	Configuration-I	17.688	17.849	17.944	17.985	18.059	18.122
		Configuration-II	17.688	18.804	19.595	19.912	20.437	20.853
	20	Configuration-I	15.538	15.640	15.707	15.738	15.796	15.850
		Configuration-II	15.538	16.184	16.624	16.798	17.085	17.314
0.17	10	Configuration-I	18.476	18.632	18.727	18.769	18.845	18.913
		Configuration-II	18.476	19.529	20.266	20.559	21.042	21.427
	20	Configuration-I	19.695	19.878	19.987	20.034	20.120	20.193
		Configuration-II	19.695	20.961	21.858	22.218	22.812	23.285
0.17	10	Configuration-I	17.776	17.903	17.990	18.032	18.112	18.190
		Configuration-II	17.776	18.568	19.118	19.339	19.707	20.009
	20	Configuration-I	20.659	20.838	20.950	21.000	21.094	21.180
		Configuration-II	20.659	21.857	22.701	23.040	23.602	24.054
50	Configuration-I	21.799	22.002	22.125	22.180	22.279	22.367	
	Configuration-II	21.799	23.192	24.183	24.581	25.242	25.771	

Table 7 First non-dimensional frequency ($\bar{\omega} = \omega(b^2/h)\sqrt{\rho_m/E_m}$) of angle-ply (45°/-45°/45°/-45°) simply supported CNTRC laminated plates with different power-law indexes, plate configurations, CNT volume fractions, and width/thickness ratios ($a/b = 1$)

f_{CNT}^*	b/h	Plate configuration	P_{in}					
			0	0.4	0.8	1.0	1.4	1.8
0.11	10	Configuration-I	19.258	19.332	19.380	19.402	19.446	19.488
		Configuration-II	19.258	19.690	19.979	20.092	20.279	20.429
	20	Configuration-I	25.892	26.049	26.049	26.179	26.252	26.318
		Configuration-II	25.892	26.897	27.582	27.853	28.296	28.646
0.14	10	Configuration-I	29.629	29.851	29.971	30.024	30.119	30.201
		Configuration-II	29.629	31.100	32.123	32.531	33.202	33.734
	20	Configuration-I	20.364	20.444	20.503	20.533	20.593	20.655
		Configuration-II	20.364	20.784	21.073	21.189	21.386	21.552
0.17	10	Configuration-I	28.218	28.389	28.493	28.540	28.631	28.715
		Configuration-II	28.218	29.277	30.002	30.290	30.765	31.147
	20	Configuration-I	32.986	33.235	33.373	33.434	33.544	33.640
		Configuration-II	32.986	34.630	35.775	36.231	36.983	37.579
0.17	10	Configuration-I	23.932	24.043	24.133	24.180	24.278	24.381
		Configuration-II	23.932	24.500	24.902	25.068	25.356	25.609
	20	Configuration-I	32.018	32.226	32.359	32.421	32.543	32.660
		Configuration-II	32.018	33.292	34.178	34.533	35.128	35.614
50	Configuration-I	36.518	36.798	36.957	37.027	37.157	37.274	
	Configuration-II	36.518	38.353	39.636	40.149	40.999	41.679	

on the vibrational behavior of CNTRC laminated plates, it is evident from Tables 6, 7, 8 and 9 that the dimensionless fundamental frequency ($\bar{\omega}$) of the plates with configurations I and II increases when P_{in} increases from 0 to 1.8. The reason for achieving these results for Configuration-I is explained by the fact that as the power-law index increases the CNT-reinforcements accumulation at both the top and bottom ply surfaces. In fact, according to the widespread thought of many researchers, this is the best way to develop high-performance polymeric FG composite structures. On the other hand, due to the special arrangement of Configuration-II, which contains two types of CNT distribution patterns (i.e., FG- Δ and FG-V), it appears that accumulating the CNTs on one surface of each ply also provides excellent results in strengthening the plates that contain several plies and exceeding even the performance of laminated plates that contain FG-X patterns. These results also confirm the main feature of FG materials, which can enhance the overall stiffness of nanocomposite structures

Table 8 First non-dimensional frequency ($\bar{\omega} = \omega(b^2/h)\sqrt{\rho_m/E_m}$) of cross-ply (0°/90°/0°/90°) simply supported CNTRC laminated plate with different power-law indexes, plate configurations, CNT volume fractions, and length/width ratios ($b/h = 10$)

f_{CNT}^*	a/b	Plate configuration	P_{in}					
			0	0.4	0.8	1.0	1.4	1.8
0.11	1.0	Configuration-I	14.359	14.454	14.512	14.538	14.586	14.629
		Configuration-II	14.359	14.980	15.403	15.569	15.839	16.053
	1.5	Configuration-I	11.309	11.387	11.434	11.455	11.494	11.529
		Configuration-II	11.309	11.823	12.174	12.313	12.538	12.716
	2.0	Configuration-I	9.692	9.699	9.710	9.717	9.731	9.746
		Configuration-II	9.692	9.699	9.710	9.717	9.731	9.748
0.14	1.0	Configuration-I	15.538	15.640	15.707	15.738	15.796	15.850
		Configuration-II	15.538	16.184	16.624	16.798	17.085	17.314
	1.5	Configuration-I	12.277	12.361	12.416	12.441	12.487	12.530
		Configuration-II	12.277	12.816	13.175	13.191	13.227	13.268
	2.0	Configuration-I	9.865	9.878	9.897	9.909	9.935	9.964
		Configuration-II	9.865	9.877	9.897	9.909	9.936	9.967
0.17	1.0	Configuration-I	17.776	17.903	17.990	18.032	18.112	18.190
		Configuration-II	17.776	18.568	19.118	19.339	19.707	20.009
	1.5	Configuration-I	13.992	14.096	14.166	14.199	14.262	14.322
		Configuration-II	13.992	14.647	15.102	15.284	15.588	15.836
	2.0	Configuration-I	12.126	12.150	12.189	12.212	12.266	12.328
		Configuration-II	12.126	12.149	12.189	12.213	12.268	12.333

Table 9 First non-dimensional frequency ($\bar{\omega} = \omega(b^2/h)\sqrt{\rho_m/E_m}$) of angle-ply (45°/-45°/45°/-45°) simply supported CNTRC laminated plates with different power-law indexes, plate configurations, CNT volume fractions, and length/width ratios ($b/h = 10$)

f_{CNT}^*	a/b	Plate configuration	P_{in}					
			0	0.4	0.8	1.0	1.4	1.8
0.11	1.0	Configuration-I	19.258	19.332	19.380	19.402	19.446	19.488
		Configuration-II	19.258	19.690	19.979	20.092	20.279	20.429
	1.5	Configuration-I	14.856	14.922	14.963	14.982	15.018	15.052
		Configuration-II	14.856	15.255	15.523	15.629	15.801	15.939
	2.0	Configuration-I	12.972	13.033	13.069	13.086	13.118	13.147
		Configuration-II	12.972	13.342	13.592	13.690	13.851	13.978
0.14	1.0	Configuration-I	20.364	20.444	20.503	20.533	20.593	20.655
		Configuration-II	20.364	20.784	21.073	21.189	21.386	21.552
	1.5	Configuration-I	15.841	15.912	15.961	15.985	16.033	16.080
		Configuration-II	15.841	16.238	16.509	16.617	16.798	16.948
	2.0	Configuration-I	13.897	13.962	14.005	14.027	14.068	14.109
		Configuration-II	13.897	14.269	14.524	14.625	14.795	14.934
0.17	1.0	Configuration-I	23.932	24.043	24.133	24.180	24.278	24.381
		Configuration-II	23.932	24.500	24.902	25.068	25.356	25.609
	1.5	Configuration-I	18.436	18.531	18.602	18.638	18.712	18.788
		Configuration-II	18.436	18.955	19.318	19.466	19.719	19.936
	2.0	Configuration-I	16.085	16.171	16.233	16.264	16.326	16.391
		Configuration-II	16.085	16.564	16.898	17.034	17.265	17.462

by adjusting the distribution of the nano-reinforcements across the plate thickness. From these observations, it can be concluded that the nonlinear distributions of nano-reinforcements along the thickness of the plies, as may emerge in the manufacturing process as a source of uncertainty, also have a considerable effect on the stiffness of CNTRC plate structures.

3.2.5 Effect of number of plies

The influence of the number of plies together with the plate configuration and power-law index on the $\bar{\omega}$ parameter of simply supported CNTRC laminated plates for cross-ply (0°/90°/0°/90°) and angle-ply (45°/-45°/45°/-45°) stacking sequences are examined in Table 10. In the analysis, the following parameter values are chosen $f_{CNT}^* = 0.11$, $b/h = 10$ and $a/b = 1$. By increasing the number of plies (n), the parameter $\bar{\omega}$

Table 10 First non-dimensional frequency ($\bar{\omega} = \omega(b^2/h)\sqrt{\rho_m/E_m}$) of simply supported cross-ply $(0^\circ/90^\circ)_n$ and angle-ply $(45^\circ/-45^\circ)_n$ CNTRC laminated plates with different number of plies, power-law indexes, and plate configurations ($b/h = 50$; $a/b = 1$; $f_{CNT}^* = 0.11$)

stacking sequence	n	Plate configuration	P _{in}					
			0	0.4	0.8	1.0	1.4	1.8
$(0^\circ/90^\circ)_n$	1	[X-X] _n	11.340	12.197	12.832	13.092	13.530	13.884
		[Λ-V] _n	11.340	10.988	10.599	10.425	10.126	9.887
	2	[X-X] _n	17.688	17.849	17.944	17.985	18.059	18.122
		[Λ-V] _n	17.688	18.804	19.595	19.912	20.437	20.853
	4	[X-X] _n	18.922	18.980	18.990	18.995	19.007	19.020
		[Λ-V] _n	18.922	19.463	19.842	19.995	20.248	20.450
6	[X-X] _n	19.139	19.180	19.175	19.174	19.176	19.179	
	[Λ-V] _n	19.139	19.503	19.753	19.854	20.023	20.158	
$(45^\circ/-45^\circ)_n$	1	[X-X] _n	19.029	20.232	21.099	21.451	22.040	22.513
		[Λ-V] _n	19.029	18.579	18.061	17.826	17.422	17.097
	2	[X-X] _n	29.629	29.851	29.971	30.024	30.119	30.201
		[Λ-V] _n	29.629	31.100	32.123	32.531	33.202	33.734
	4	[X-X] _n	32.186	32.273	32.281	32.286	32.301	32.317
		[Λ-V] _n	32.186	32.908	33.405	33.605	33.936	34.200
	6	[X-X] _n	32.764	32.829	32.817	32.814	32.814	32.819
		[Λ-V] _n	32.764	33.254	33.584	33.718	33.942	34.121

largely increases for both plate configurations. For $P_{in} \neq 0$, it can be seen that when $n = 1$, the plates with [X-X]_n arrangement yield the largest $\bar{\omega}$ while the plates with [Λ-V]_n arrangement produce the smallest $\bar{\omega}$. However, when $n = 2, 4$ and 6 , the highest first non-dimensional frequency parameter $\bar{\omega}$ characterizes the plate with [Λ-V]_n arrangement and the smallest one parameter goes to characterizes the plate with [X-X]_n arrangement. It can be concluded from this analysis that the best way to enhance the laminated plate structural performance containing 4, 8, or 12 plies of CNTRC is to put the FG-Λ distribution patterns in the lower half of the laminated plate and to put the FG-V distribution patterns in its upper half and accumulate the CNTs to the exterior surfaces of plies.

3.2.6 Effect of P_{in} on the first eight non-dimensional frequencies

The first eight non-dimensional frequencies versus the power-law index of CNTRC cross-ply $(0^\circ/90^\circ/0^\circ/90^\circ)$ and angle-ply $(45^\circ/-45^\circ/45^\circ/-45^\circ)$ laminated plates are plotted in Figs. 5 and 6, respectively. The SSSS and CCCC boundary conditions are considered in this study, where b/h , a/b , and f_{CNT}^* are set to be 50, 1, and 0.11, respectively. The obtained results reveal that increasing the power-law index leads to an increase in the first eight non-dimensional frequencies for the two types of boundary conditions, the staking sequences and the plate configurations. Indeed, one can see that the influence of the power-law index on the first eight $\bar{\omega}$ parameters can be better observed for the laminated plates with Configuration-II. In other words, the observations reveal that when P_{in} increases, the gap between the first eight non-dimensional frequencies corresponding to the plate with Configuration-I is too small compared to those of the plate with Configuration-II. Moreover, it can be observed that the fully clamped and fully simply supported plates provide the highest and lowest values of the first eight non-dimensional frequencies, respectively.

3.2.7 Effect of CNTs orientation angle

Figure 7 shows the effects of CNTs orientation angle (θ), plate configuration, power-law index, and CNT volume fraction on the non-dimensional fundamental frequency ($\bar{\omega}$) of SSSS and CCCC angle-ply $(\theta/\theta/\theta/-\theta)$ CNTRC laminated plates. In the analysis, b/h and a/b are taken equal to 10 and 1, respectively. For the considered values of θ , one can observe that the fundamental frequency curves present symmetric increase and decrease with respect to the line of $\theta = 45^\circ$; in other words, Fig. 7 shows that the $\bar{\omega}$ parameter of the CNTRC laminated plates increases from 15° to 45° , and decreases from 45° to 75° for different values of CNT volume fractions, plate configurations, and boundary conditions.

The effects of CNTs orientation angle, power-law index, plate configuration, and width/thickness ratio on the non-dimensional fundamental frequency ($\bar{\omega}$) parameter of SSSS and CCCC CNTRC laminated plates

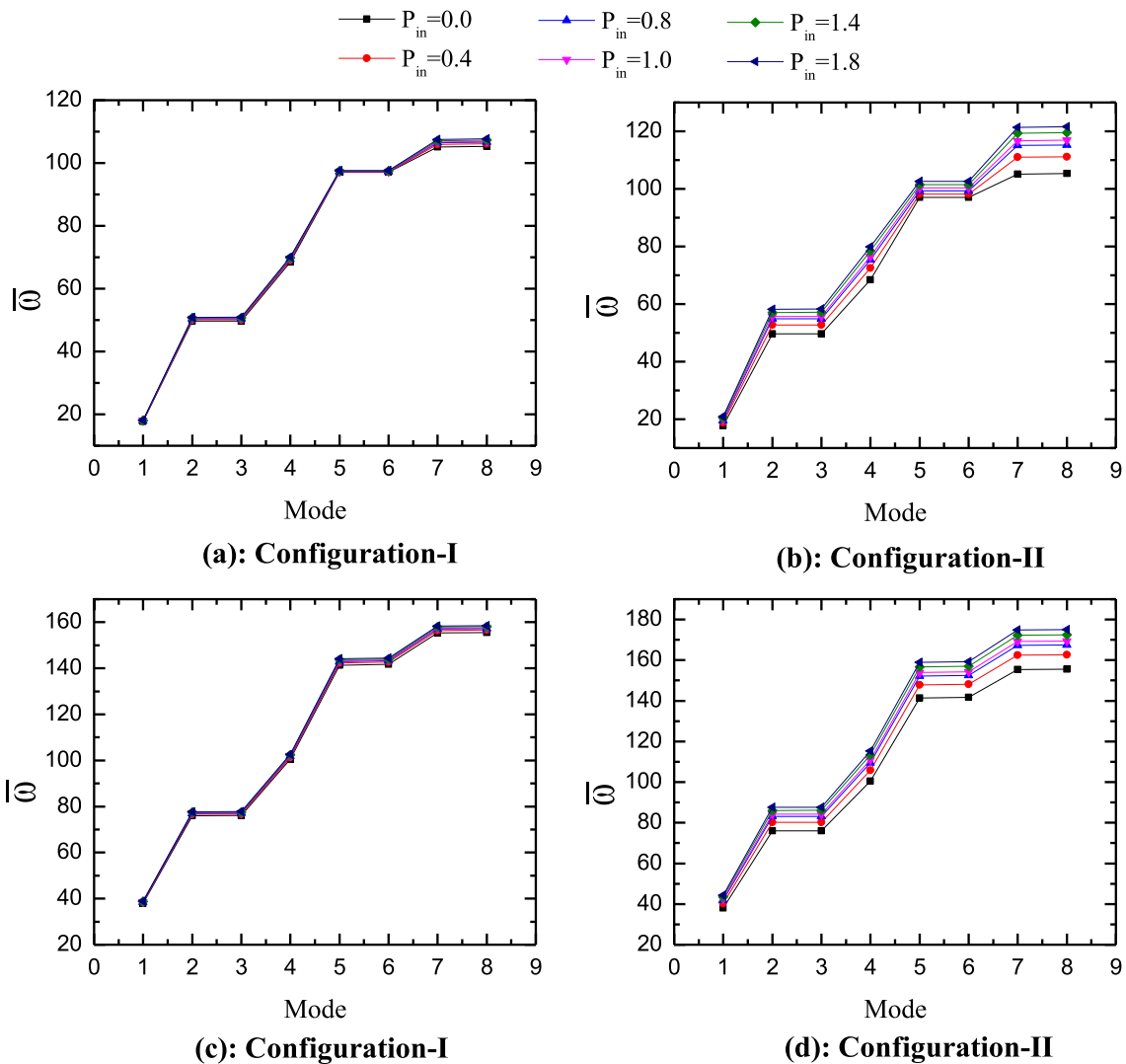


Fig. 5 Effect of power-law index and plate configuration on the first eight non-dimensional $\bar{\omega}$ parameters of cross-ply ($0^\circ/90^\circ/0^\circ/90^\circ$) CNTRC laminated plates for different boundary conditions: **a & b** SSSS; **c & d** CCCC ($f_{CNT}^* = 0.11$, $a/b = 1$; $b/h = 50$)

are depicted in Fig. 8. In this modeling, a/b and f_{CNT}^* are taken to be equal to 1 and 0.11, respectively. It is obvious that the results of Fig. 7 can be discerned again, i.e., the fundamental frequency varies symmetrically on either side of the line of $\theta = 45^\circ$. In contrast, this trend is reversed for thinner ($b/h = 50$) CCCC CNTRC laminated plates, where the $\bar{\omega}$ parameter decreases and increases when θ varies from 15° to 45° and from 45° to 75° , respectively, as depicted in Fig. 8f.

The effects of CNTs orientation angle, power-law index, plate configuration, and different values of length/width ratio on the $\bar{\omega}$ parameter of SSSS and CCCC CNTRC laminated plates are plotted in Fig. 9, for $b/h = 10$ and $f_{CNT}^* = 0.11$. It can be seen that the curves of the plate fundamental frequencies with $a/b = 1$ vary symmetrically with respect to the line of $\theta = 45^\circ$, while the curves of the fundamental frequencies corresponding to the plates with $a/b = 1.5$ and $a/b = 2.0$, increase with the increase of angle θ to become almost unchanged when θ increases from 60° to 75° . In addition to the above observations, the results illustrated in Figs. 7, 8 and 9 indicate that the stiffening effect of the plates with Configuration-II overtakes that of Configuration-I for all values of CNTs orientation angle.

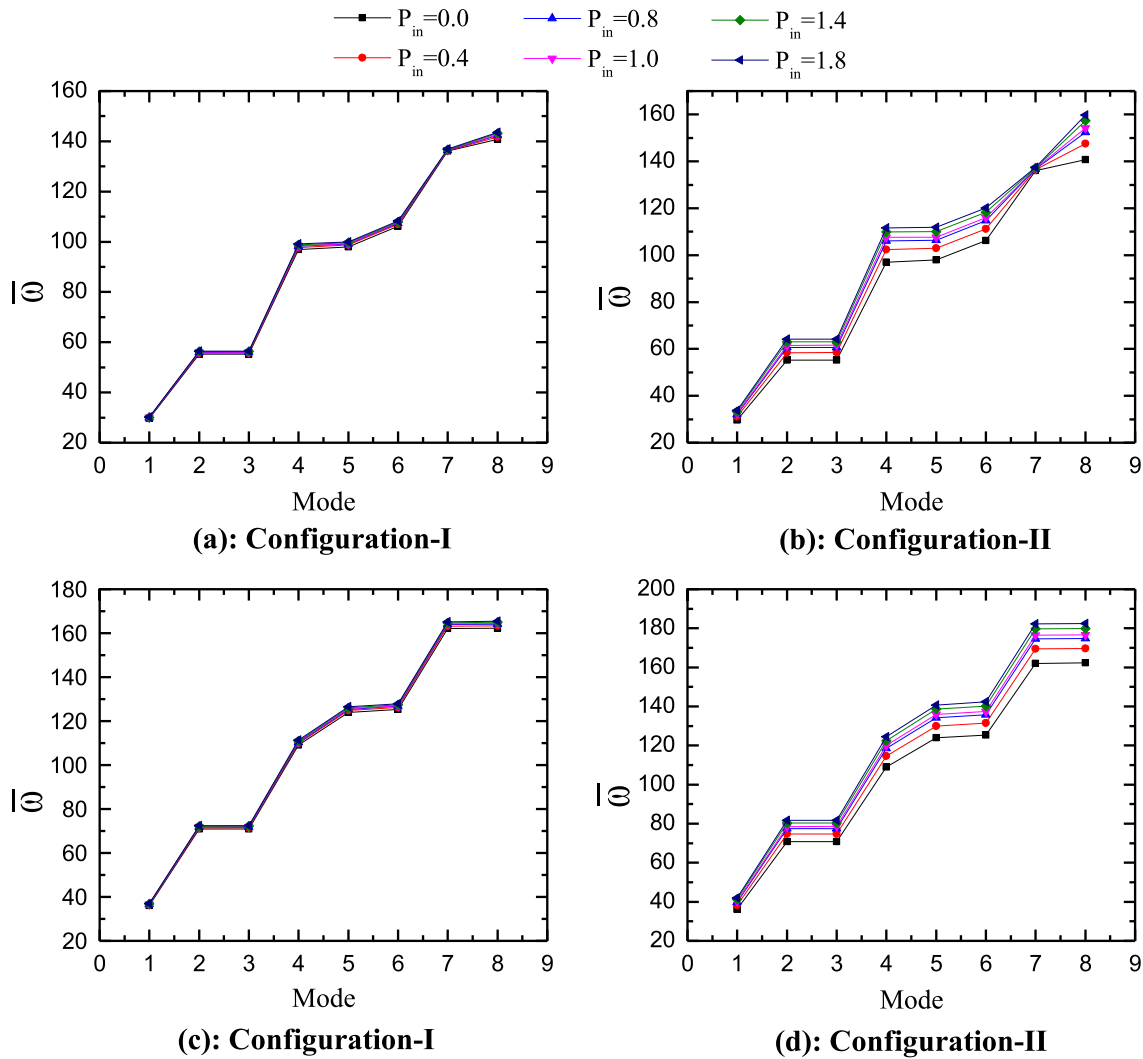


Fig. 6 Effect of power-law index and plate configuration on the first eight non-dimensional $\bar{\omega}$ parameters of angle-ply ($45^\circ/ -45^\circ/45^\circ/ -45^\circ$) CNTRC laminated plates for different boundary conditions: **a & b** SSSS; **c & d** CCCC ($f_{CNT}^* = 0.11$, $a/b = 1$; $b/h = 50$)

3.2.8 Effect of the plate boundary conditions

The combined effects of plate configuration, power-law index, and various combinations of boundary conditions on the fundamental non-dimensional frequency $\bar{\omega}$ parameter are examined in Table 11. The combinations of boundary conditions considered are shown in Fig. 10, for which S denotes simply supported, C clamped and F free. In this analysis, b/h , a/b and f_{CNT}^* are taken equal to 10, 1, and 0.11, respectively. As can be seen from Table 11, within every single boundary condition combination, the $\bar{\omega}$ parameter increases as P_{in} increases for both plates configurations I and II. However, for $P_{in} \neq 0$, it is evident that plates with configuration-II are more affected by P_{in} than those with Configuration-I for all the considered boundary conditions. The obtained frequencies are arranged in Table 11 from highest to lowest for the different combinations of boundary conditions. One can conclude that the more the plate edges are restrained (from free to simply supported, then to clamped), the higher the fundamental frequencies.

3.2.9 Discussion on the mode shapes

Let us now consider a square CNTRC laminated plate with $b/h = 20$, $f_{CNT}^* = 0.11$, and SSSS boundary conditions. The angle-ply $(\theta/ -\theta/ \theta/ -\theta)$ stacking sequence and the Configuration-II layout arrangement are

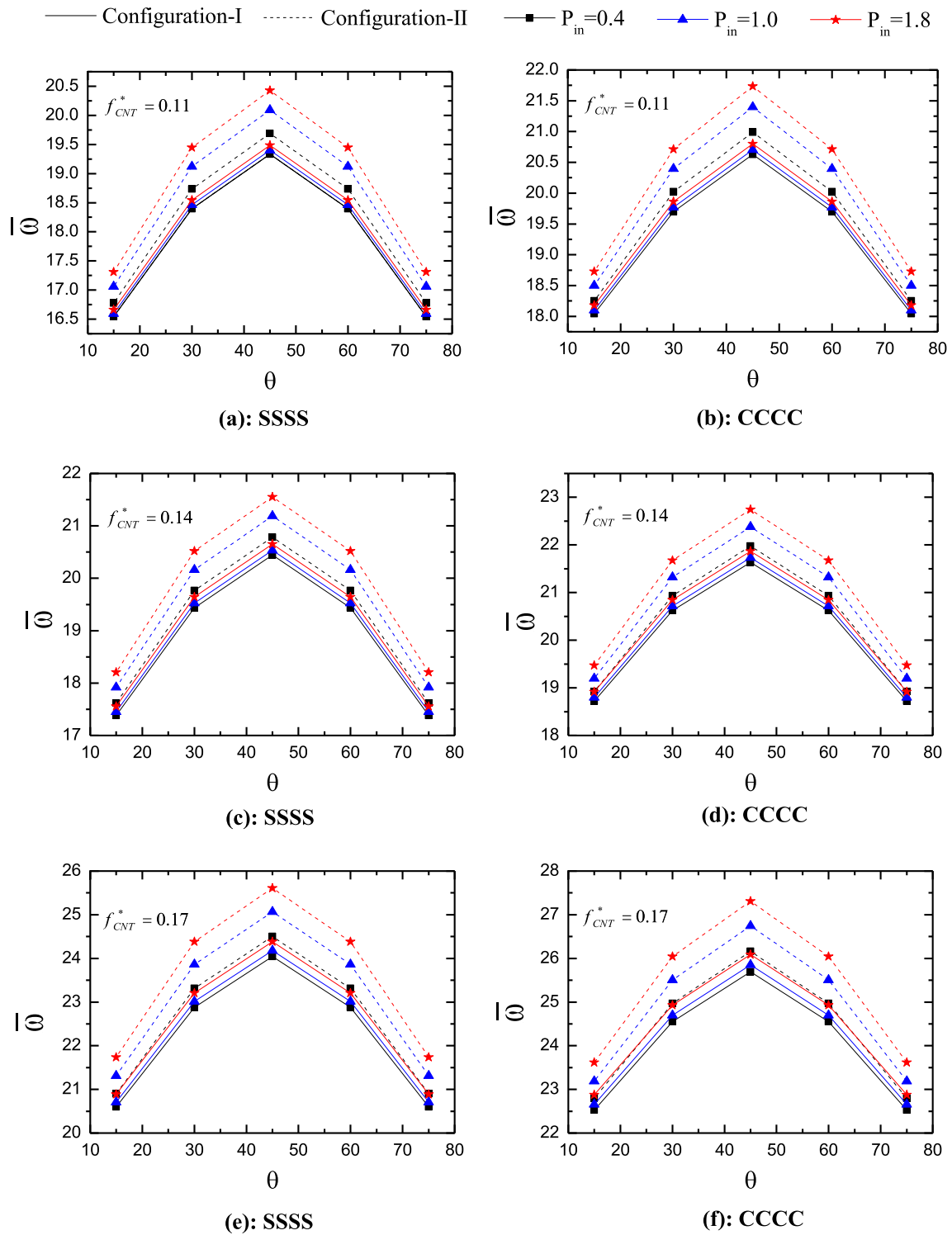


Fig. 7 Effects of CNTs orientation angle θ , power-law index, CNT volume fraction, and plate configuration on the $\bar{\omega}$ parameter of SSSS and CCCC angle-ply ($\theta / -\theta / \theta / -\theta$) CNTRC laminated plates ($a/b = 1$; $b/h = 10$)

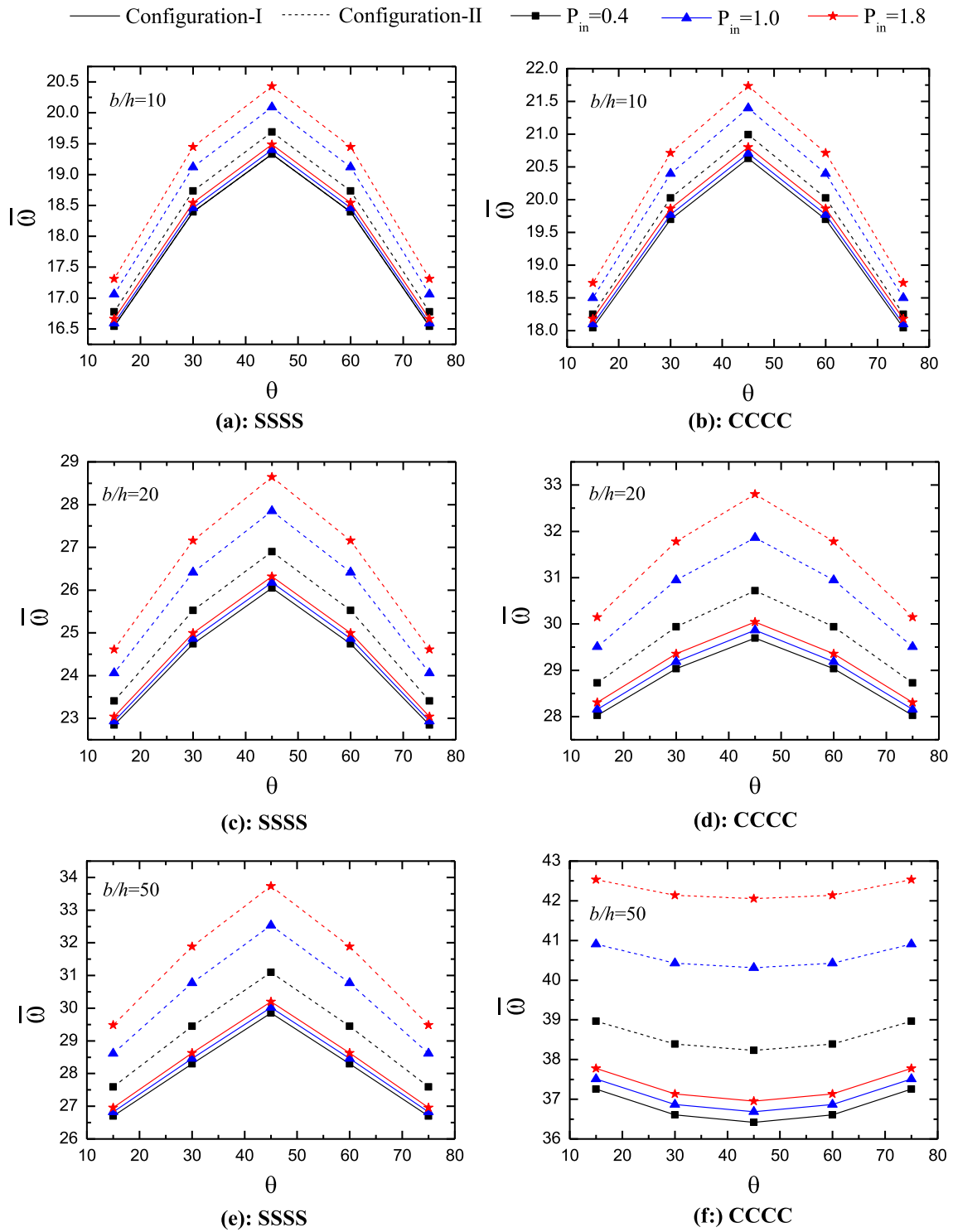


Fig. 8 Effect of CNTs orientation angle θ , power-law index, CNT volume fraction, and plate configuration on the first $\bar{\omega}$ parameter of SSSS and CCCC angle-ply ($\theta / -\theta / \theta / -\theta$) CNTRC laminated plates ($f_{CNT}^* = 0.11$; $a/b = 1$)

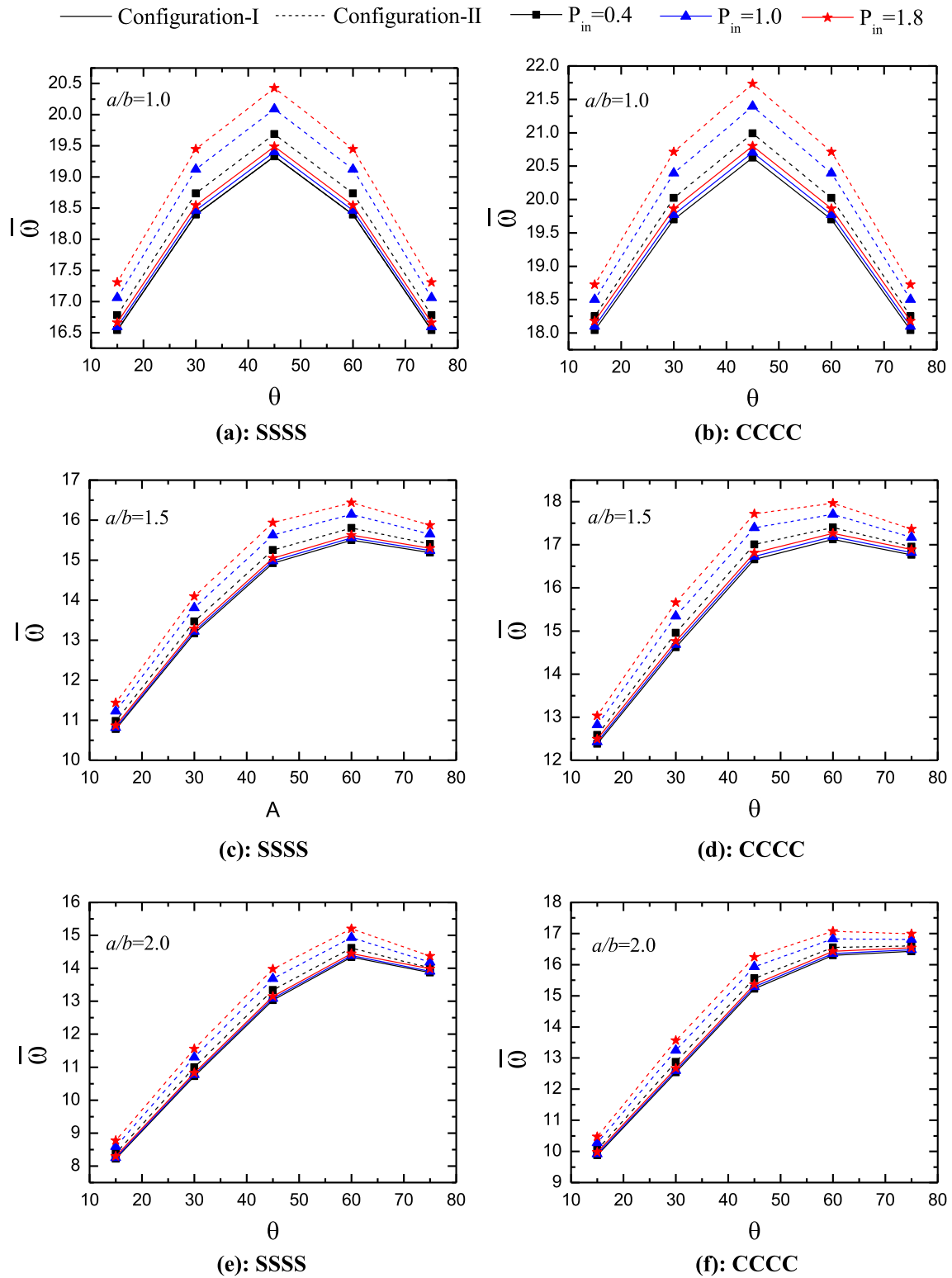


Fig. 9 Effect of CNTs orientation angle θ , power-law index, CNT volume fraction, and plate configuration on the first $\bar{\omega}$ parameter of SSSS and CCCC angle-ply ($\theta / -\theta / \theta / -\theta$) CNTRC laminated plates ($f_{CNT}^* = 0.11$; $b/h = 10$)

Table 11 First non-dimensional frequency ($\bar{\omega} = \omega(b^2/h)\sqrt{\rho_m/E_m}$) of cross-ply ($0^\circ/90^\circ/0^\circ/90^\circ$) CNTRC laminated plates with various boundary conditions, and power-law indexes ($b/h = 10$; $a/b = 1$; $f_{CNT}^* = 0.11$)

Boundary conditions	plate configuration	P_{in}					
		0.0	0.4	0.8	1.0	1.4	1.8
CCCC	Configuration-I	21.309	21.381	21.433	21.457	21.506	21.553
	Configuration-II	21.309	21.714	21.981	22.085	22.256	22.395
CCCS	Configuration-I	19.633	19.709	19.761	19.786	19.834	19.880
	Configuration-II	19.633	20.081	20.377	20.493	20.683	20.835
CCSS	Configuration-I	18.137	18.217	18.270	18.295	18.342	18.387
	Configuration-II	18.137	18.623	18.950	19.079	19.290	19.374
CSCS	Configuration-I	17.801	17.883	17.938	17.963	18.010	18.055
	Configuration-II	17.801	18.303	18.637	18.767	18.979	19.148
CSSS	Configuration-I	16.171	16.258	16.314	16.339	16.387	16.430
	Configuration-II	16.171	16.723	17.095	17.241	17.479	17.668
CCCF	Configuration-I	15.567	15.624	15.664	15.683	15.719	15.755
	Configuration-II	15.567	15.897	16.117	16.204	16.346	16.461
CCFF	Configuration-I	14.827	14.873	14.907	14.923	14.955	14.987
	Configuration-II	14.827	15.078	15.243	15.307	15.414	15.502
SSSS	Configuration-I	14.359	14.454	14.512	14.538	14.586	14.629
	Configuration-II	14.359	14.980	15.403	15.569	15.839	16.053
FSSC	Configuration-I	12.816	12.873	12.911	12.928	12.962	12.993
	Configuration-II	12.816	13.159	13.386	13.474	13.619	13.734
SSCF	Configuration-I	11.396	11.467	11.512	11.532	11.568	11.601
	Configuration-II	11.396	11.860	12.176	12.300	12.503	12.664

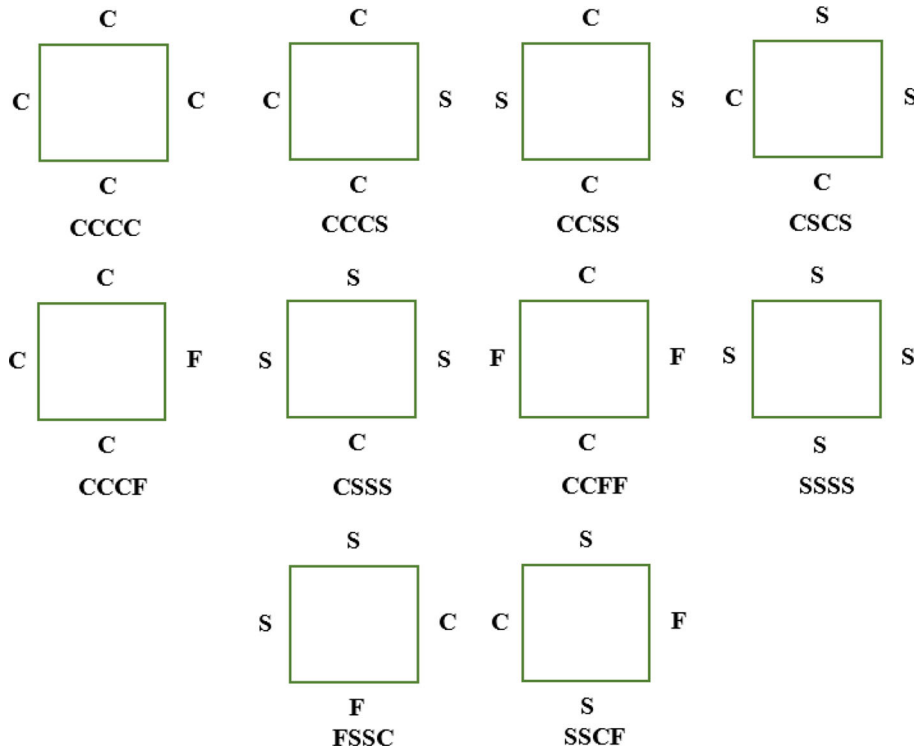


Fig. 10 Boundary conditions combinations

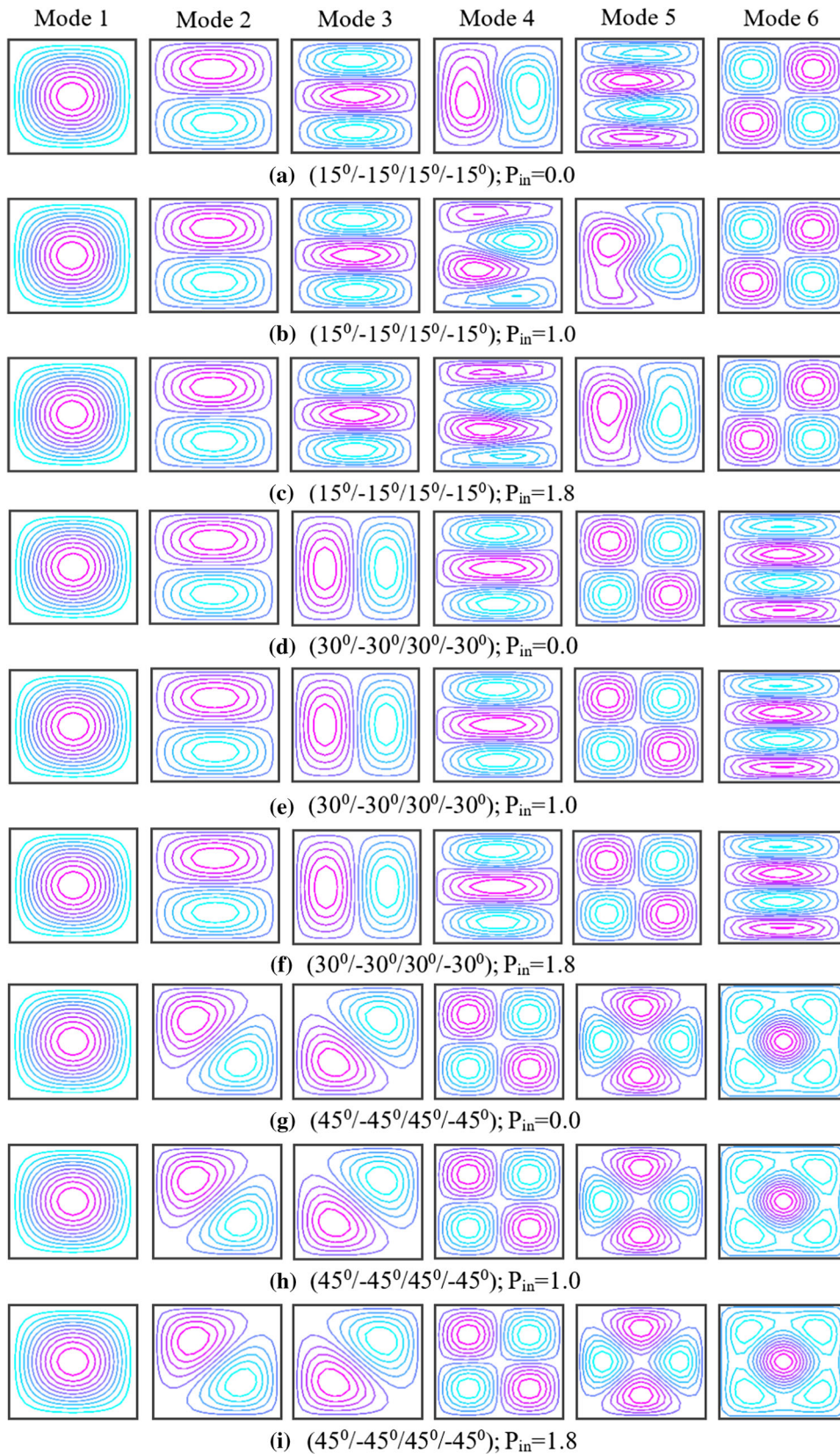


Fig. 11 Contour curves of the first six mode shapes of square simply supported angle-play $[\theta/-\theta/\theta/-\theta]$ CNTRC laminated plate. (Configuration-II, $b/h = 20$, $f_{CNT}^* = 0.11$)

chosen in this analysis, which aims to study the dependency of the plate mode shapes in terms of contour curves on the in-plane CNTs orientation angle θ and the power-law index P_{in} . The contour curves of the first six mode shapes related to the associated natural mode shapes are depicted in Fig. 11 for three values of CNTs orientation angle ($\theta = 15^\circ$, $\theta = 30^\circ$, and $\theta = 45^\circ$) and three levels of power-law indexes ($P_{in} = 0.0$, $P_{in} = 1.0$, and $P_{in} = 1.8$). From Fig. 11, it is discernible that the increase in P_{in} does not make any change in the mode shapes, except when θ is equal to 15° (cases (a), (b), and (c)), where mode interchange is observed: Mode 4 in case (a) tends to be Mode 5 in cases (b) and (c), while Mode 5 in case (a) tends to be Mode 4 in cases (b) and (c). On the other hand, it is clear that the mode shapes of the CNTRC laminated plate are highly affected by the reinforcement orientation angle, this aspect can be observed by comparing cases characterized by different values of θ , but have the same values of P_{in} (case (a), case (d), and case (g), for instance).

4 Conclusion

The free vibration response of multi-layer functionally graded carbon nanotube-reinforced composite laminated plates using the finite element method was analyzed in this paper. The homogenization of each ply was done via the extended rule of mixture. Kinematic relations were obtained employing Lagrange's equations and the first-order shear deformation theory. Focusing on the effect of the linear and nonlinear distribution forms of the nano-reinforcements based CNTs and the plate configuration, the numerical results obtained show the influence of several parameters, including the effects of (i) number of ply layers, (ii) CNT volume fractions and distribution patterns, (iii) geometry of the plate, (iv) ply orientation angle, (v) number of plies and (vi) boundary conditions on the free vibration behavior of CNTRC laminated plates. The following points summarize the most crucial findings of the present study:

- The minimum number of ply layers needed to produce accurate predictions for free vibration response of CNTRC plates is 20 layers per ply.
- The natural frequencies of the CNTRC laminated plates can be amplified by using a greater volume fraction of CNTs.
- The use of high width/thickness ratios can increase the natural frequency of the CNTRC laminated plate structure, while high aspect ratios can weaken it.
- The appropriate strengthening way for FG-CNTRC laminated plates that contain more than four plies, is to put the FG- Λ patterns in the lower half of the laminated plates and the FG-V patterns in their upper half.
- Natural frequencies of the CNTRC laminated plates that contain FG-X or both FG- Λ and FG-V patterns can be increased when CNTs fillers are accumulated to the lateral surfaces of the plies.
- The orientation angle of CNTs and the number of plies have a remarkable influence on the natural frequencies of the CNTRC laminated plates, as discussed in Sect. 3.2.7.
- Plate structures with fully clamped boundary conditions yield larger natural frequencies than plates with fully simply supported boundary conditions.

References

1. Papageorgiou, D.G., Li, Z., Liu, M., Kinloch, I.A., Young, R.J.: Mechanisms of mechanical reinforcement by graphene and carbon nanotubes in polymer nanocomposites. *Nanoscale* **12**, 2228–2267 (2020)
2. Mao, Y., He, Q., Zhao, X.: Designing complex architected materials with generative adversarial networks. *Sci. Adv.* **6**, eaaz4169 (2020)
3. Griebel, M., Hamaekers, J.: Molecular dynamics simulations of the elastic moduli of polymer–carbon nanotube composites. *Comput. Methods Appl. Mech. Eng.* **193**, 1773–1788 (2004)
4. Han, Y., Elliott, J.: Molecular dynamics simulations of the elastic properties of polymer/carbon nanotube composites. *Comput. Mater. Sci.* **39**, 315–323 (2007)
5. Esawi, A.M.K., Farag, M.M.: Carbon nanotube reinforced composites: potential and current challenges. *Mater. Des.* **28**, 2394–2401 (2007)
6. Godara, A., Mezzo, L., Luizi, F., Warriar, A., Lomov, S.V., Van Vuure, A.W., Gorbatikh, L., Moldenaers, P., Verpoest, I.: Influence of carbon nanotube reinforcement on the processing and the mechanical behaviour of carbon fiber/epoxy composites. *Carbon N. Y.* **47**, 2914–2923 (2009)
7. De Volder, M.F.L., Tawfik, S.H., Baughman, R.H., Hart, A.J.: Carbon nanotubes: Present and future commercial applications. *Science* **339**, 535–539 (2013)
8. Thostenson, E.T., Ren, Z., Chou, T.-W.: Advances in the science and technology of carbon nanotubes and their composites: a review. *Compos. Sci. Technol.* **61**, 1899–1912 (2001)
9. Kim, M., Park, Y.-B., Okoli, O.I., Zhang, C.: Processing, characterization, and modeling of carbon nanotube-reinforced multiscale composites. *Compos. Sci. Technol.* **69**, 335–342 (2009)

10. Spitalsky, Z., Tasis, D., Papagelis, K., Galiotis, C.: Carbon nanotube–polymer composites: Chemistry, processing, mechanical and electrical properties. *Prog. Polym. Sci.* **35**, 357–401 (2010)
11. Kaseem, M., Hamad, K., Ko, Y.G.: Fabrication and materials properties of polystyrene/carbon nanotube (PS/CNT) composites: a review. *Eur. Polym. J.* **79**, 36–62 (2016)
12. Qian, D., Dickey, E.C., Andrews, R., Rantell, T.: Load transfer and deformation mechanisms in carbon nanotube–polystyrene composites. *Appl. Phys. Lett.* **76**, 2868–2870 (2000)
13. Liew, K.M., Pan, Z., Zhang, L.-W.: The recent progress of functionally graded CNT reinforced composites and structures. *Sci. China Physics, Mech. Astron.* **63**, 234601 (2020)
14. Attia, M.A., Shanab, R.A.: On the dynamic response of bi-directional functionally graded nanobeams under moving harmonic load accounting for surface effect. *Acta Mech.* **233**, 3291–3317 (2022)
15. Deshpande, G.A., Kulkarni, S.: Free vibration analysis of functionally graded plates under uniform and linear thermal environment. *Acta Mech.* **230**, 1347–1354 (2019)
16. Ecsedi, I.: Non-uniform torsion of functionally graded anisotropic bar of an elliptical cross section. *Acta Mech.* **231**, 2947–2953 (2020)
17. Falsone, G., La Valle, G.: A homogenized theory for functionally graded Euler-Bernoulli and Timoshenko beams. *Acta Mech.* **230**, 3511–3523 (2019)
18. Bourihane, O., Mhada, K., Sitli, Y.: New finite element model for the stability analysis of a functionally graded material thin plate under compressive loadings. *Acta Mech.* **231**, 1587–1601 (2020)
19. Shen, H.-S.: Nonlinear bending of functionally graded carbon nanotube-reinforced composite plates in thermal environments. *Compos. Struct.* **91**, 9–19 (2009)
20. Wu, Z., Zhang, Y., Yao, G.: Nonlinear forced vibration of functionally graded carbon nanotube reinforced composite circular cylindrical shells. *Acta Mech.* **231**, 2497–2519 (2020)
21. Jeong, H., Cho, J.-R.: Study on the detailed and homogenized models for functionally graded carbon nanotube-reinforced composite beams. *J. Mech. Sci. Technol.* **35**, 4085–4092 (2021)
22. Liu, Z., Wang, C., Duan, G., Tan, J.: Isogeometric analysis of functionally graded CNT-reinforced composite plates based on refined plate theory. *J. Mech. Sci. Technol.* **34**, 3687–3700 (2020)
23. Civalek, O., Jalaei, M.H.: Buckling of carbon nanotube (CNT)-reinforced composite skew plates by the discrete singular convolution method. *Acta Mech.* **231**, 2565–2587 (2020)
24. Zhang, L.W.: An element-free based IMLS-Ritz method for buckling analysis of nanocomposite plates of polygonal planform. *Eng. Anal. Bound. Elem.* **77**, 10–25 (2017)
25. Zhang, L.W., Liew, K.M., Reddy, J.N.: Postbuckling of carbon nanotube reinforced functionally graded plates with edges elastically restrained against translation and rotation under axial compression. *Comput. Methods Appl. Mech. Eng.* **298**, 1–28 (2016)
26. Ansari, R., Torabi, J., Shakouri, A.H.: Vibration analysis of functionally graded carbon nanotube-reinforced composite elliptical plates using a numerical strategy. *Aerosp. Sci. Technol.* **60**, 152–161 (2017)
27. Thai, C.H., Tran, T.D., Phung-Van, P.: A size-dependent moving Kriging meshfree model for deformation and free vibration analysis of functionally graded carbon nanotube-reinforced composite nanoplates. *Eng. Anal. Bound. Elem.* **115**, 52–63 (2020)
28. Zhang, L.W., Lei, Z.X., Liew, K.M.: Free vibration analysis of functionally graded carbon nanotube-reinforced composite triangular plates using the FSDT and element-free IMLS-Ritz method. *Compos. Struct.* **120**, 189–199 (2015)
29. Zhang, L.W., Lei, Z.X., Liew, K.M.: Vibration characteristic of moderately thick functionally graded carbon nanotube reinforced composite skew plates. *Compos. Struct.* **122**, 172–183 (2015)
30. Zhang, L.W.: On the study of the effect of in-plane forces on the frequency parameters of CNT-reinforced composite skew plates. *Compos. Struct.* **160**, 824–837 (2017)
31. Lei, Z.X., Zhang, L.W., Liew, K.M.: Vibration of FG-CNT reinforced composite thick quadrilateral plates resting on Pasternak foundations. *Eng. Anal. Bound. Elem.* **64**, 1–11 (2016)
32. Quoc, T.H., Van Tham, V., Tu, T.M.: Active vibration control of a piezoelectric functionally graded carbon nanotube-reinforced spherical shell panel. *Acta Mech.* **232**, 1005–1023 (2021)
33. Zhang, Y., Liu, W.: Nonlinear vibration response of a functionally graded carbon nanotube-reinforced composite conical shell using a stress function method. *Acta Mech.* **233**, 3157–3174 (2022)
34. Ansari, R., Torabi, J., Hassani, R.: A comprehensive study on the free vibration of arbitrary shaped thick functionally graded CNT-reinforced composite plates. *Eng. Struct.* **181**, 653–669 (2019)
35. Cho, J.-R.: Buckling analysis of sandwich plates with FG-CNTRC layers by natural element hierarchical models. *J. Mech. Sci. Technol.* **36**, 1949–1957 (2022)
36. Wang, Z.-X., Shen, H.-S.: Nonlinear vibration and bending of sandwich plates with nanotube-reinforced composite face sheets. *Compos. Part B Eng.* **43**, 411–421 (2012)
37. Yang, J., Huang, X.-H., Shen, H.-S.: Nonlinear vibration of temperature-dependent FG-CNTRC laminated plates with negative Poisson's ratio. *Thin-Walled Struct.* **148**, 106514 (2020)
38. García-Macías, E., Castro-Triguero, R., Friswell, M.I., Adhikari, S., Sáez, A.: Metamodel-based approach for stochastic free vibration analysis of functionally graded carbon nanotube reinforced plates. *Compos. Struct.* **152**, 183–198 (2016)
39. Poursmaeeli, S., Fazlzadeh, S.A., Ghavanloo, E., Marzocca, P.: Uncertainty propagation in vibrational characteristics of functionally graded carbon nanotube-reinforced composite shell panels. *Int. J. Mech. Sci.* **149**, 549–558 (2018)
40. Mirjavadi, S.S., Afshari, B.M., Barati, M.R., Hamouda, A.M.S.: Nonlinear free and forced vibrations of graphene nanoplatelet reinforced microbeams with geometrical imperfection. *Microsyst. Technol.* **25**, 3137–3150 (2019)
41. Vo-Duy, T., Truong, T.T., Nguyen-Quang, K., Nguyen-Thoi, T., Vu-Do, H.C.: A type of novel nonlinear distributions for improving significantly the stiffness of carbon nanotube-reinforced composite beams. *Int. J. Comput. Methods.* **17**, 1950057 (2020)
42. Tornabene, F., Fantuzzi, N., Baccocchi, M., Viola, E.: Effect of agglomeration on the natural frequencies of functionally graded carbon nanotube-reinforced laminated composite doubly-curved shells. *Compos. Part B Eng.* **89**, 187–218 (2016)

43. Fantuzzi, N., Tornabene, F., Baccocchi, M., Dimitri, R.: Free vibration analysis of arbitrarily shaped Functionally Graded Carbon Nanotube-reinforced plates. *Compos. Part B Eng.* **115**, 384–408 (2017)
44. Jiao, P., Chen, Z., Ma, H., Zhang, D., Ge, P.: Buckling analysis of thin rectangular FG-CNTRC plate subjected to arbitrarily distributed partial edge compression loads based on differential quadrature method. *Thin-Walled Struct.* **145**, 106417 (2019)
45. Garcia-Macias, E., Rodriguez-Tembleque, L., Saez, A.: Bending and free vibration analysis of functionally graded graphene vs. carbon nanotube reinforced composite plates. *Compos. Struct.* **186**, 123–138 (2018)
46. Chiker, Y., Bachene, M., Guemana, M., Attaf, B., Rechak, S.: Free vibration analysis of multilayer functionally graded polymer nanocomposite plates reinforced with nonlinearly distributed carbon-based nanofillers using a layer-wise formulation model. *Aerosp. Sci. Technol.* **104**, 105913 (2020)
47. Chiker, Y., Bachene, M., Bouaziz, S., Guemana, M., Amar, M.B., Haddar, M.: Free vibration analysis of hybrid laminated plates containing multilayer functionally graded carbon nanotube-reinforced composite plies using a layer-wise formulation. *Arch. Appl. Mech.* **91**, 463–485 (2020)
48. Tran, H.Q., Tran, M.T., Nguyen-Tri, P.: A new four-variable refined plate theory for static analysis of smart laminated functionally graded carbon nanotube reinforced composite plates. *Mech. Mater.* **142**, 103294 (2020)
49. Lei, Z.X., Zhang, L.W., Liew, K.M.: Buckling analysis of CNT reinforced functionally graded laminated composite plates. *Compos. Struct.* **152**, 62–73 (2016)
50. Chakraborty, S., Dey, T., Kumar, R.: Stability and vibration analysis of CNT-Reinforced functionally graded laminated composite cylindrical shell panels using semi-analytical approach. *Compos. Part B Eng.* **168**, 1–14 (2019)
51. Arani, A.G., Kiani, F., Afshari, H.: Free and forced vibration analysis of laminated functionally graded CNT-reinforced composite cylindrical panels. *J. Sandw. Struct. Mater.* **23**, 255–278 (2019)
52. Nguyen-Quang, K., Vo-Duy, T., Dang-Trung, H., Nguyen-Thoi, T.: An isogeometric approach for dynamic response of laminated FG-CNT reinforced composite plates integrated with piezoelectric layers. *Comput. Methods Appl. Mech. Eng.* **332**, 25–46 (2018)
53. Fu, T., Chen, Z., Yu, H., Wang, Z., Liu, X.: Mechanical behavior of laminated functionally graded carbon nanotube reinforced composite plates resting on elastic foundations in thermal environments. *J. Compos. Mater.* **53**, 1159–1179 (2019)
54. Huu Quoc, T., Minh Tu, T., Van Tham, V.: Free vibration analysis of smart laminated functionally graded CNT reinforced composite plates via new four-variable refined plate theory. *Materials (Basel)* **12**, 3675 (2019)
55. Malekzadeh, P., Zarei, A.R.: Free vibration of quadrilateral laminated plates with carbon nanotube reinforced composite layers. *Thin-Walled Struct.* **82**, 221–232 (2014)
56. Malekzadeh, P., Heydarpour, Y.: Mixed Navier-layerwise differential quadrature three-dimensional static and free vibration analysis of functionally graded carbon nanotube reinforced composite laminated plates. *Meccanica* **50**, 143–167 (2015)
57. Zhang, L.W., Selim, B.A.: Vibration analysis of CNT-reinforced thick laminated composite plates based on Reddy's higher-order shear deformation theory. *Compos. Struct.* **160**, 689–705 (2017)
58. Lei, Z.X., Zhang, L.W., Liew, K.M.: Free vibration analysis of laminated FG-CNT reinforced composite rectangular plates using the kp-Ritz method. *Compos. Struct.* **127**, 245–259 (2015)
59. Huang, B., Guo, Y., Wang, J., Du, J., Qian, Z., Ma, T., Yi, L.: Bending and free vibration analyses of antisymmetrically laminated carbon nanotube-reinforced functionally graded plates. *J. Compos. Mater.* **51**, 3111–3125 (2017)
60. Fidelus, J.D., Wiesel, E., Gojny, F.H., Schulte, K., Wagner, H.D.: Thermo-mechanical properties of randomly oriented carbon/epoxy nanocomposites. *Compos. Part A Appl. Sci. Manuf.* **36**, 1555–1561 (2005)
61. Zhu, P., Lei, Z.X., Liew, K.M.: Static and free vibration analyses of carbon nanotube-reinforced composite plates using finite element method with first order shear deformation plate theory. *Compos. Struct.* **94**, 1450–1460 (2012)
62. Zhang, C.-L., Shen, H.-S.: Temperature-dependent elastic properties of single-walled carbon nanotubes: Prediction from molecular dynamics simulation. *Appl. Phys. Lett.* **89**, 81904 (2006)
63. Saiah, B., Bachene, M., Guemana, M., Chiker, Y., Attaf, B.: On the free vibration behavior of nanocomposite laminated plates contained piece-wise functionally graded graphene-reinforced composite plies. *Eng. Struct.* **253**, 113784 (2022)
64. Reddy, J.N.: *Mechanics of laminated composite plates and shells: theory and analysis*. CRC Press (2003)
65. Matsunaga, H.: Free vibration and stability of functionally graded plates according to a 2-D higher-order deformation theory. *Compos. Struct.* **82**, 499–512 (2008)

Publisher's Note Springer Nature remains neutral with regard to jurisdictional claims in published maps and institutional affiliations.

Springer Nature or its licensor (e.g. a society or other partner) holds exclusive rights to this article under a publishing agreement with the author(s) or other rightsholder(s); author self-archiving of the accepted manuscript version of this article is solely governed by the terms of such publishing agreement and applicable law.